

Optimization of Ribbed Helicopter Panel Design

Team 3
Ryan Campbell
Jeremiah Dwight
Gregory Hutchins
Nicholas Kemme

Abstract

The purpose of this optimization analysis was to improve on the design of a helicopter engine panel with the introduction of beveled ribs. A 0.5 m x 0.5 m sheet was examined for four different variables: number of ribs, height of ribs, width of ribs, and thickness of panel. These variables were altered to optimize four different objectives: maximize fundamental natural frequency, maximize heat rejection, and minimize maximum stress experienced subject to a wind load, and minimize maximum stress subject to an impact load. These four optimizations were performed independently of each other initially, and then a full system optimization was performed, in which pareto-optimal surfaces were generated. ANSYS was used for all modeling and optimization.

Submodel optimizations were all successful in improving the performance of the panel over a plain, flat-panel design. Thermal performance improved the least, while the other performance characteristics improved over 600%.

The system optimization demonstrated that a utopia point does not exist; that is, no panel design will simultaneously optimize all four objective functions. Instead, pareto-optimal surfaces show the tradeoffs between the objectives. These surfaces could be used to make a decision on the design of the panel for its application based on relative weights of the objective functions.

Acknowledgements

The team would like to thank Dr. Max Ren for his patience and dedication to helping the team understand the concepts behind this project. In addition, the team appreciates the availability of Arizona State University's resources for this project. Without the High Performance Computing Lab and the Goldwater Computing Lab, this project would not have been possible.

Table of Contents

Acknowledgements	2
Table of Contents	3
1. Introduction	5
2. Nomenclature	6
3. Mathematical Models	7
3.1. Objective Functions	7
3.2. Design Variables	7
3.3. Constraints	8
3.4. Optimization Problems	9
3.4.1. Modal	9
3.4.2. Thermal	10
3.4.3. Strength	10
3.4.4. Impact Strength	10
4. Simulation Setup	11
4.1. Engineering Data	11
4.2. Geometry	11
4.3. Mesh	12
4.4. Boundary Conditions and Loads	12
4.4.1. Modal	13
4.4.2. Thermal	13
4.4.3. Strength	13
4.4.4. Impact Strength	14
5. Submodel Optimization Process	15
5.1. Design of Experiments	16
5.2. Metamodel	16
5.3. Response Surface Optimization	16
6. Submodel Optimization Results	17
6.1. Modal	17
6.1.1. Initial Design Performance	17
6.1.2. Parametric Study	18
6.1.3. Optimized Design	20
6.1.4. Response Surface, Sensitivity, and Convergence	21
6.2. Thermal	25
6.2.1. Initial Design Performance	25
6.2.2. Parametric Study	25
6.2.3. Optimized Design	27
6.2.4. Response Surface, Sensitivity, and Convergence	28
6.3. Strength	31
6.3.1. Initial Design Performance	31
6.3.2. Parametric Study	32
6.3.3. Optimized Design	33
6.3.4. Response Surface, Sensitivity, and Convergence	34

6.4. Impact Strength	36
6.4.1. Initial Design Performance	36
6.4.2. Parametric Study	37
6.4.3. Optimized Design	39
6.4.4. Response Surface, Sensitivity, and Convergence	41
7. System Optimization	44
7.1. Process	44
7.2. Results	44
8. Conclusions	47
9. References	48
10. Appendix	49

1 Introduction

Currently, helicopter engine cover panels are a flat sheet of metal, with the only alteration being some raised or cut out vents for heat release is placed over the component it is meant to house as seen in Figure 1.1.



Figure 1.1. Helicopter Engine Cover Panel

This optimization examines the addition of raised ribs to the panel by indenting the existing flat panel to create the raised ribs, an idea that originated from a similar study done by Yang, et al. [1]. This structure could be accomplished using only one additional manufacturing process that would press the existing panel onto a mold to bend it into the desired geometry. This modification is intended to aid in heat rejection, fundamental natural frequency, and strength of the panel for both the typical wind pressure against the panel as well as impact. The outer dimensions of the panel will not be variable and has been simplified for original proof of concept that this study will examine from a typical panel's slightly curved geometry to a flat panel of similar size (0.5m x 0.5m). The initial design of the ANSYS model with 7 ribs can be seen in Figure 1.2 below.

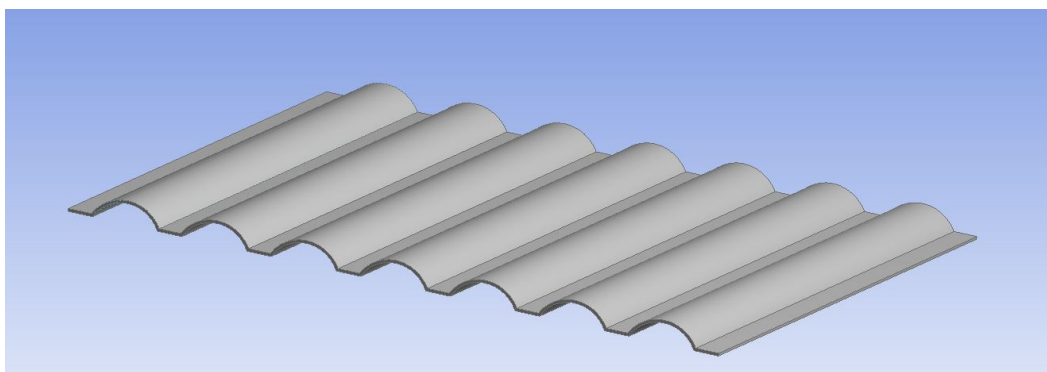


Figure 1.2: ANSYS model of helicopter engine panel with 7 ribs

2 Nomenclature

The nomenclature for all submodels, including design variables, geometric constants, and objective functions, is shown in Table 2.1 below. These symbols are described in more detail in the subsequent sections.

Table 2.1. Nomenclature for all submodels.

Symbol	Description	Unit	Type
h	height of ribs	m	Variable
w	width of ribs	m	Variable
N	number of ribs	--	Variable
t	thickness of panel (uniform)	m	Variable
d	distance between ribs	m	Constant
W	width of panel	m	Constant
L	length of panel	m	Constant
ω	fundamental natural frequency	Hz	Objective
$T_{surf,avg}$	average surface temperature	°C	Objective
$\sigma_{max,wind}$	maximum stress from wind load	Pa	Objective
$\sigma_{max,impact}$	maximum stress from impact load	Pa	Objective

3 Mathematical Models

3.1 Objective Functions

In accordance with the problem statements above, the panel design is to be optimized with respect to four unique objective functions: maximize fundamental natural frequency, minimize average surface temperature, maximize wind load strength, and maximize impact strength. Each of these objective functions is a function of the design variables, though these relationships are highly complex. Since ANSYS is used for simulations, it is unnecessary to formulate the analytic relationships between the objective functions and design variables. Instead, the objective functions and design variables are related implicitly, as shown in Section 3.4.

3.2 Design Variables

Four design variables are chosen to optimize the design of the panel. These are listed in Table 3.2.1 and shown in Figure 3.2.1. These variables are the same for all submodels.

Table 3.2.1. Design variables.

Symbol	Description
w	width of ribs
h	height of ribs
t	thickness of panel (uniform)
N	number of ribs



Figure 3.2.1. Design variables and other parameters.

3.3 Constraints

The spacing between the ribs and on either end of the rib series were constrained to be equal to one another and limited to a maximum value d (15 mm) to ensure the panel had enough flat space to be riveted to the helicopter frame and/or adjacent panels. For fixed total width W of the panel (0.5 m), this leads to a constraint on the maximum width of each rib:

$$w \leq \frac{1}{N} [W - d(N + 1)]$$

Since the upper bound for w is dependent on the number of ribs, a table was created and referenced for optimizations of panels with N ribs:

Table 3.3.1. Upper bound of w based on N .

N	w (mm)	N	w (mm)
1	470	11	29
2	228	12	25
3	147	13	22
4	106	14	20
5	82	15	17
6	66	16	15
7	54	17	14
8	46	18	12
9	39	19	11
10	34	20	9

Furthermore, the width should always be greater than some reasonably small value, which was chosen to be 5 mm. The number of ribs is constrained to be between 1 and 20 ribs. To allow for the case where the optimal design has 0 ribs, the lower bound of height is set to 0 mm, while the upper limit is set to 30 mm so that the ribs do not protrude significantly from the aircraft, as this might significantly affect aerodynamics. An additional constraint on the rib height is that it should not exceed half the width of the rib, since this would create a concave rib shape. (Concave ribs could not be manufactured by pressing cylinders into the sheet metal, which is the manufacturing method with which this project is concerned.) The thickness is limited to manufacturable values between gauge 18 (1.024 mm) and gauge 9 (2.906 mm); hence, it is a discrete domain given by the following table [2]:

Table 3.3.2. Discrete domain of t.

Gauge (AWG)	t (mm)	Gauge (AWG)	t (mm)
9	2.906	14	1.628
10	2.588	15	1.450
11	2.304	16	1.290
12	2.052	17	1.151
13	1.829	18	1.024

These constraints can be written mathematically as shown below:

$$\begin{aligned}
 5mm \leq w &\leq \frac{1}{N} [W - d(N + 1)] \\
 0 \leq h &\leq 30mm \\
 h &\leq \frac{1}{2}w \\
 t &\in [1.024, 1.151, \dots, 2.906]mm \\
 N &\in [1, 20]
 \end{aligned}$$

3.4 Optimization Problems

In this section, the optimization problems are written in negative null form for each of the four submodels. Since all the constraints are the same for each submodel, the inequality constraints are written in vector form here so that they can be referenced concisely elsewhere:

$$\mathbf{g} = \begin{bmatrix} g_1 \\ g_2 \\ \vdots \\ g_5 \end{bmatrix} = \begin{bmatrix} 5mm - w \\ w - \frac{1}{N} [W - d(N + 1)] \\ -h \\ h - 30mm \\ h - \frac{1}{2}w \end{bmatrix}$$

where $d = 15$ mm and $W = 0.5$ m.

3.4.1 Modal

The fundamental natural frequency can be written as an implicit function of the design variables. Maximizing the frequency is equivalent to minimizing the negative frequency, allowing the problem to be written in negative null form as shown below.

$$\omega = f(w, h, t, N)$$

$$\begin{aligned} \min \quad & -f \\ \text{s.t.} \quad & \mathbf{g} \leq 0 \\ & t \in \{1.024, \dots, 2.906\} \text{mm} \\ & N \in \{1, 2, \dots, 20\} \end{aligned}$$

3.4.2 Thermal

The average surface temperature of the panel can be written as an implicit function of the design variables. This function is then minimized subject to the constraints defined above.

$$T_{surf,avg} = f(w, h, t, N)$$

$$\begin{aligned} \min \quad & f \\ \text{s.t.} \quad & \mathbf{g} \leq 0 \\ & t \in \{1.024, \dots, 2.906\} \text{mm} \\ & N \in \{1, 2, \dots, 20\} \end{aligned}$$

3.4.3 Strength

Maximizing the panel's wind load strength is equivalent to minimizing the maximum stress in the panel. The maximum stress in the panel can be written as an implicit function of the design variables. This function is then minimized subject to the constraints defined above.

$$\sigma_{max,wind} = f(w, h, t, N)$$

$$\begin{aligned} \min \quad & f \\ \text{s.t.} \quad & \mathbf{g} \leq 0 \\ & t \in \{1.024, \dots, 2.906\} \text{mm} \\ & N \in \{1, 2, \dots, 20\} \end{aligned}$$

3.4.4 Impact Strength

Maximizing the panel's impact strength is equivalent to minimizing the maximum stress in the panel subject to an impact load. This can again be written as an implicit function of the design variables. This function is then minimized subject to the constraints defined above.

$$\sigma_{max,impact} = f(w, h, t, N)$$

$$\begin{aligned} \min \quad & f \\ \text{s.t.} \quad & \mathbf{g} \leq 0 \\ & t \in \{1.024, \dots, 2.906\} \text{mm} \\ & N \in \{1, 2, \dots, 20\} \end{aligned}$$

4 Simulation Setup

All simulations and optimization were performed using ANSYS Workbench. Modal was used for modal analysis, Steady State Thermal for thermal analysis, Static Structural for wind load strength analysis, and Explicit Dynamics for impact strength analysis.

4.1 Engineering Data

Since 7075-T6 aluminum is a typical material of choice for helicopters, this was the same material chosen for this project's application. ANSYS already has a general "Aluminum Alloy" material in its material library, and these properties are quite close to those of 7075-T6 aluminum; hence, this was the material selected for simulations. The engineering data for this material is shown in Table 4.1.1 below.

Table 4.1.1. Engineering data used for simulations.

Property	Value
Density	2770 kg/m ³
Coefficient of thermal expansion (at 22°C)	23 μm/m·°C
Young's modulus	71 GPa
Poisson's ratio	0.33
Bulk modulus	69.6 GPa
Shear modulus	26.7 GPa
Specific heat capacity	875 J/kg·°C
Engine bay air temperature	900°C
Ambient temperature	22°C

4.2 Geometry

A CAD model of the panel was created by drawing a 2D sketch of the panel cross-section (perpendicular to the ribs) as shown in Figure 3.2.1. First a single series lines and arcs were drawn. This series was then offset above the base series so that, if the base series arcs were semicircles, the overall rib shape would remain convex. (Concave ribs could not be manufactured by pressing cylinders into the sheet metal, which is the manufacturing method with which this project is concerned.)

The dimensions for the initial design of the panel are given in Table 4.2.1 below.

Table 4.2.1. Dimensions of initial panel design.

Parameter	Value
w	50 mm
h	10 mm
t	2.5 mm
N	4

This profile was extruded a depth equal to the total width of the panel so that its shape from the top is square ($0.5\text{m} \times 0.5\text{m}$). Since images of the geometry are available elsewhere in the report, none is shown here.

Fillets were considered for the edges where the ribs meet the flat part of the panel. However, analysis showed negligible changes in simulation results for all objective functions when fillets were added (surprisingly, the edges were not the locations of maximum stress). Therefore, fillets were left out of the panel in order to maintain a simpler mesh and lower computation time.

4.3 Mesh

As with all FEA models, a mesh is created to discretize the model for numerical calculation of the solution. If the mesh is too coarse, the solution will not be accurate. Conversely, if the mesh is too fine, it will take an unnecessarily long time to solve the simulation; this compounds for an optimization problem, where many simulations are required to generate the design points for the metamodel (discussed in Section 5).

For this project, all submodels were run with the following parameters, which balanced accuracy of the solution with reasonable computation time. Figure 4.3.1 shows an image of the meshed model and the details of the mesh parameters.

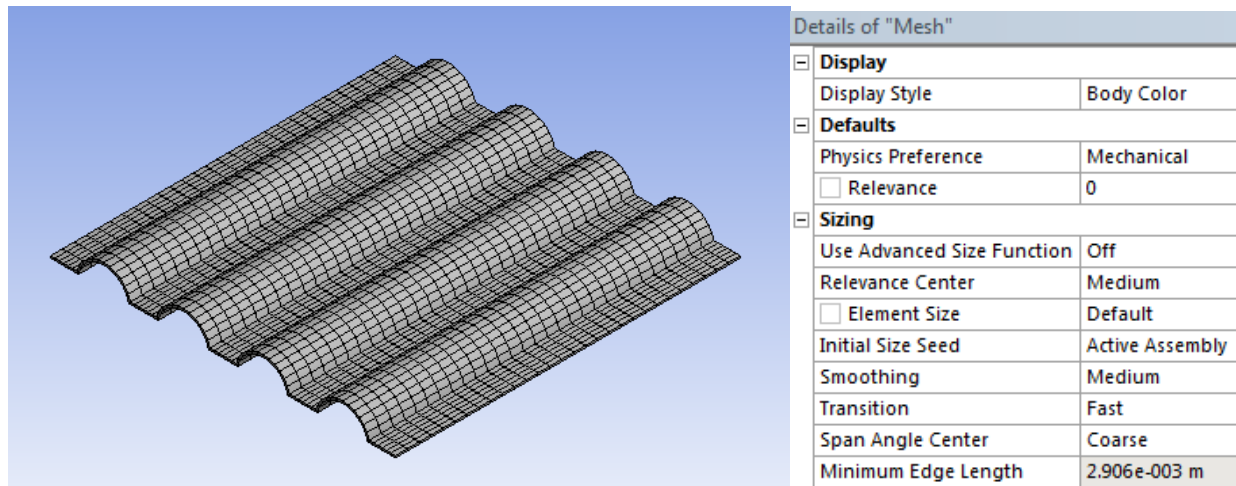


Figure 4.3.1. Meshed model and mesh parameters.

4.4 Boundary Conditions and Loads

For each sub-model, the same boundary conditions were used. Though in reality the panel would likely be riveted along its outer edges, this ANSYS model was simplified to reduce simulation time and thereby make the optimization feasible. Hence, the four outer faces of the

panel were modeled as fixed supports, as shown below in Figure 4.4.1. The loads varied between the sub-models.

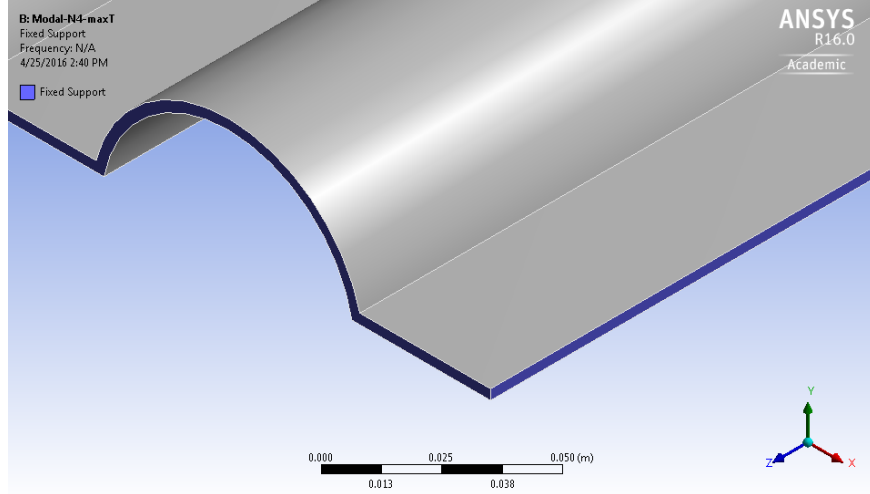


Figure 4.4.1. Boundary conditions (fixed supports).

4.4.1 Modal

Natural frequency examines the undamped modal response. This means no loads are applied to the panel. Instead, only boundary conditions are used, as described above.

4.4.2 Thermal

Steady state thermal examines a geometry's properties based on applied loads with the assumption that the loads are consistent and that the system is modeled at steady state. In addition to constant thermal loadings, this means that no mountings are needed and no external forces are accounted for. A convection film coefficient and ambient temperature were applied to each side of the plate to simulate exposure to the hot air inside the engine compartment and the rapidly flowing air outside of the aircraft. The film coefficient inside was 500 W/m² at an ambient temperature of 900°C while a film coefficient of 1,000 W/m² and an ambient temperature of 22°C was used for the outside of the helicopter. This takes into account the high thermal loads presented by the plate being in close proximity to the jet turbine and high wind speeds across the plate due to the rotors. These values were estimated based on prior thermodynamic experience and to provide a clear distinction between the two environments.

4.4.3 Strength

The wind pressure of basic speed is given by the equation $q = \frac{V^2}{383.6}$ where V is the velocity in mph and q is the pressure in PSF. Maximum (worst case) wind speeds are approximately 200 mph for this project's applications because of the higher speeds created by

the helicopter's blades. From this the team found that the pressure on the panel in SI units would be approximately 4950 Pa. This load was applied as a uniform pressure over all the top surfaces of the panel.

4.4.4 Impact Strength

The examined impact situation was desired to mimic an impact that the helicopter may take in the air, such as a bird hitting the panel. For simplicity, this bird was modeled as a sphere with a diameter of 20 mm. This diameter was chosen due to the 28 mm wingspan of a common pigeon and resulting estimated equivalent volume. Literature review also determined the weight and Young's modulus of a bird's bone, assumed to be its most structurally stiff and heaviest components, to be 20 g and 20 GPa respectively [3]. A calculation of a volume of a sphere complimented with the equation to determine density from mass and volume produced a density of 4.7747 kg/m^3 . The sphere was positioned such that it was 0.03 m above the top face of the panel to ensure that even if the rib height constraint was active, the bird would not have already impacted the panel upon initialization of the simulation. Literature reviews also revealed that the average pigeon flies at 11 m/s [4] so this was the velocity determined for the sphere modeling the bird set to impact the panel.

All previously discussed boundary conditions stated to be applicable to all sub-sections are also applicable for the impact analysis including boundary conditions, and absence of outer edge rivets.

5 Submodel Optimization Process

Direct optimization of an FEA model can be very computationally expensive. For each point, the ANSYS must run a simulation not only to evaluate the objective function at that point, but also to calculate the gradient and/or to perform a line search. Therefore, a metamodel is used to replace the actual model, and response surface optimization is performed instead of direct optimization. In brief, a response surface is created from a set of design points to approximate the objective function in the feasible domain. Then, optimization is performed on that response surface, where function and gradient information is readily available. Figure 5.1 below shows an example of the process architecture for modal analysis in ANSYS Workbench.

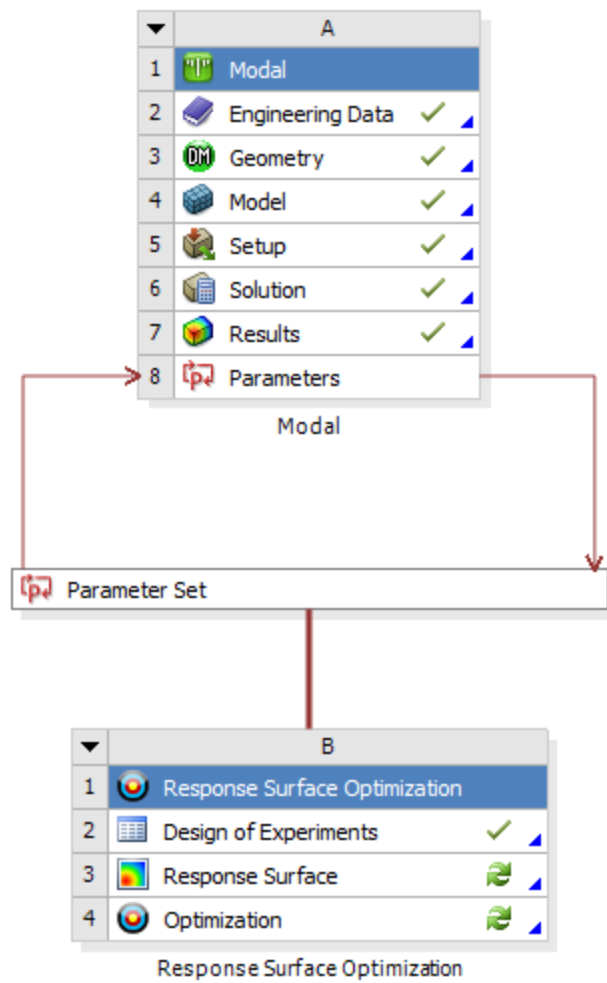


Figure 5.1. Process architecture for simulation and optimization.

5.1 Design of Experiments

The response surface requires a set of design points and their corresponding objective function values. Evaluating the objective function takes several minutes for every design point. Therefore, a Design of Experiments (DOE) is used to systematically and efficiently sample the feasible domain.

For this project, all submodels used a Latin Hypercube Sampling (LHS) scheme. This generates a set of l samples that is independent of the number of design variables. This is the primary advantage of LHS. In addition, every design point generated from LHS has unique values in every dimension, which lends to the efficiency of this scheme.

5.2 Metamodel

The design points from the DOE and their respective objective function values are used to create a response surface, which serves as a metamodel that approximates the actual behavior of the system. For this project, all submodels used a Kriging method with variable kernels, as this is a widely accepted method for creating metamodels from computer simulations. An interesting aspect of Kriging is that this method ensures that the response surface passes exactly through the sampled design points. This can eliminate the need to verify the optimization solution if the algorithm leads to a design point.

5.3 Response Surface Optimization

The response surface generated by the Kriging method is then used to search for the optimal solution to the problem. For this search, a Mixed-Integer Sequential Quadratic Programming (MISQP) method is used because it can handle non-linear, non-convex problems. Another advantage to MISQP is that it can handle discrete variables. MISQP assumes that integer variables have a smooth influence on the objective function, meaning function values do not change drastically when the variable is incremented.

After solving the problem initially, the solution is verified by running a simulation to calculate the true objective function value at that point. If the optimal solution is within 1% of the true objective function value, the optimization is terminated. Otherwise, the solution is added as another design point, the response surface is updated, and the optimization is performed again. As more and more design points are added in the vicinity of the true optimal solution, the response surface becomes more and more accurate. Eventually, the algorithm will either converge to a verified design point, or will be within 1% of the true objective function value, which is considered sufficiently accurate.

Since ANSYS cannot update the panel geometry according to a variable number of ribs, separate optimizations were run for each value of N . A binary search method was used to find the optimum number of ribs. If N^* was the optimum number of ribs, optimizations were also performed for N^*-1 and N^*+1 ribs to verify that N^* was the location of a local optimum.

6 Submodel Optimization Results

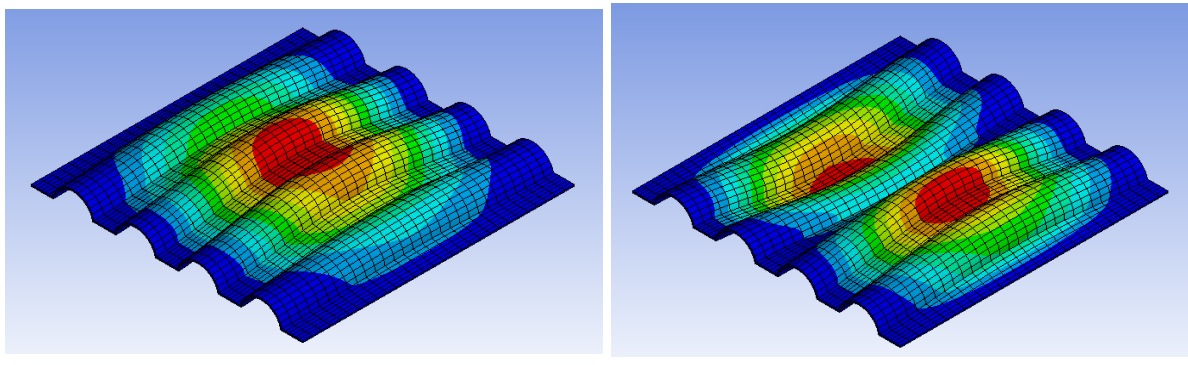
6.1 Modal

6.1.1 Initial Design Performance

The natural frequencies reported by ANSYS for the initial panel design are shown in Table 6.1.1.1 below. Figure 6.1.1.1 shows the corresponding mode shapes.

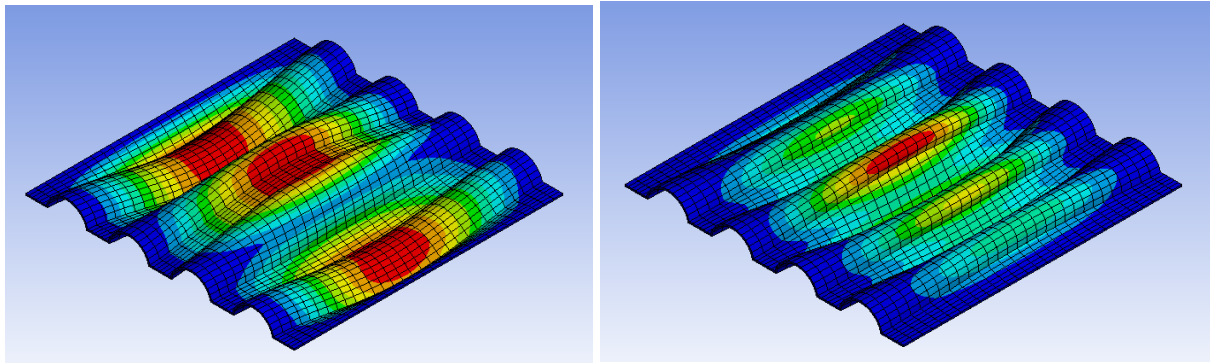
Table 6.1.1.1. Natural frequencies of optimized panel.

Mode	Frequency (Hz)
1	293.63
2	371.17
3	516.00
4	727.24
5	728.73
6	817.61

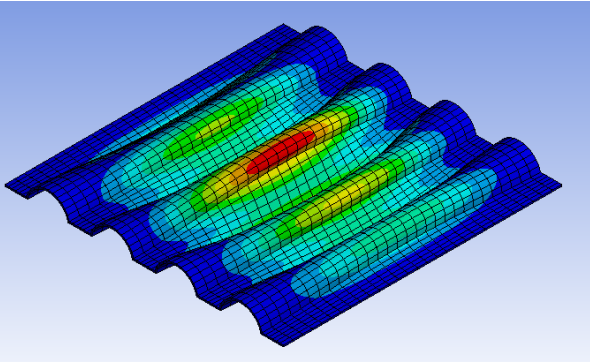


(a) Mode 1

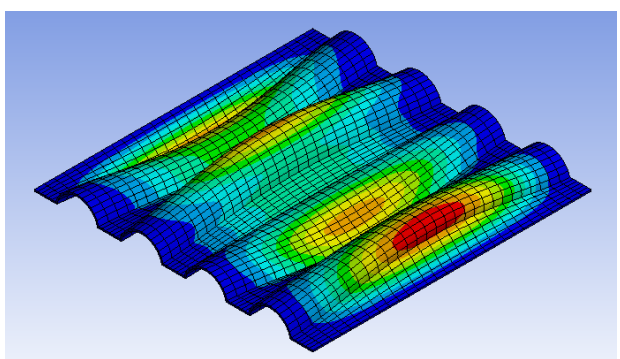
(b) Mode 2



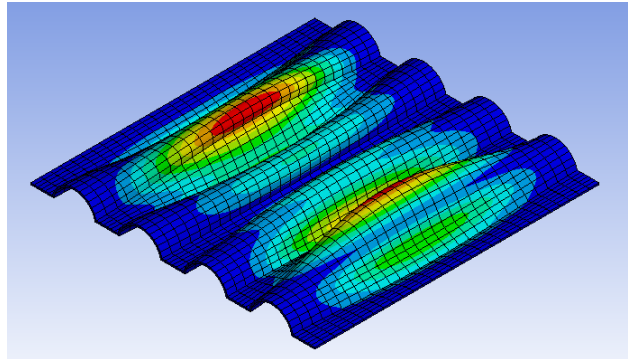
(c) Mode 3



(d) Mode 4



(e) Mode 5



(f) Mode 6

Figure 6.1.1.1. Mode shape results.

Typical helicopter engines can run at up to 20,900 RPM, which is a frequency of about 348 Hz. Since the fundamental natural frequency of the panel is below – but still in the same vicinity as – the engine frequency, the panel needs to be optimized to increase the fundamental frequency safely outside this range. Otherwise, resonance will occur, which could be structurally catastrophic for the helicopter.

6.1.2 Parametric Study

Figures 6.1.2.1 through 6.1.2.4 show the effect of w , h , t , and N on the fundamental natural frequency of the panel. (The parameters not shown on each plot are all at their optimized values.) While frequency increases monotonically with height and thickness, frequency appears to reach a global maximum at non-boundary values for width and number of ribs.

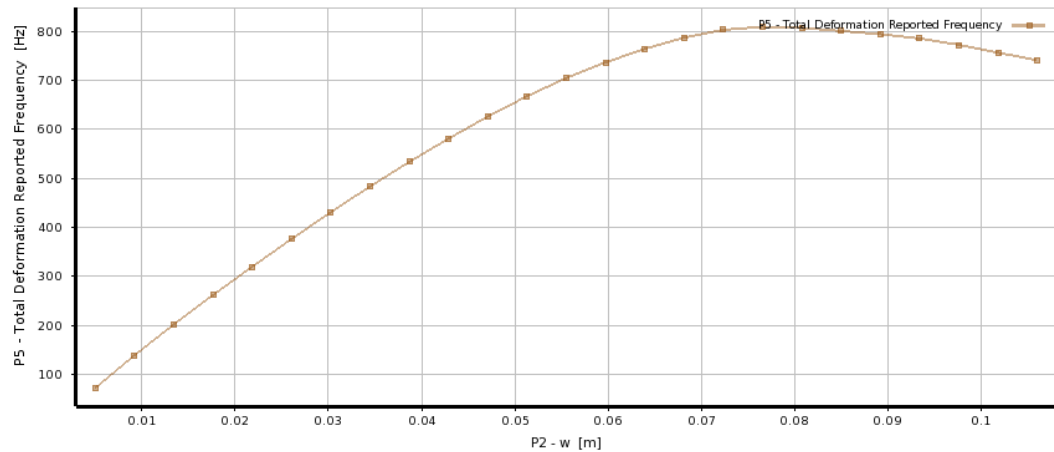


Figure 6.1.2.1. Frequency vs rib width.

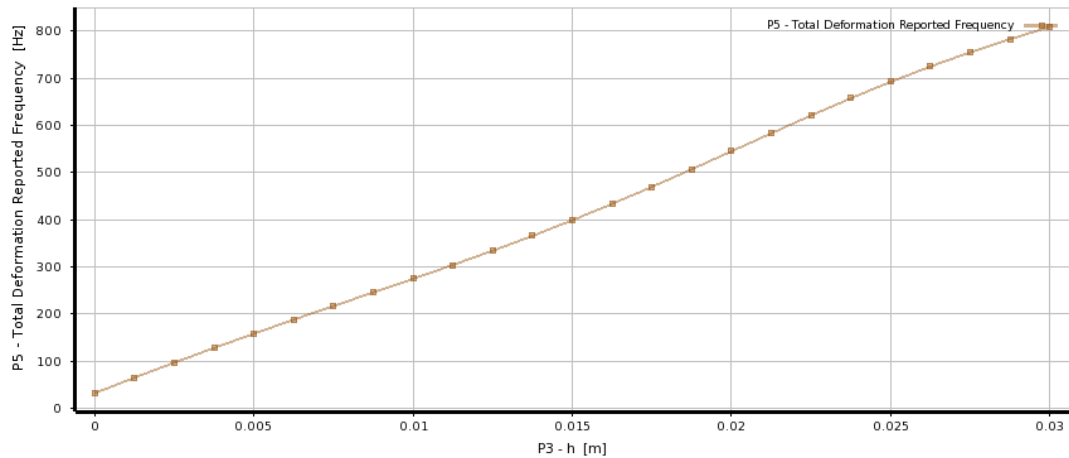


Figure 6.1.2.2. Frequency vs rib height.

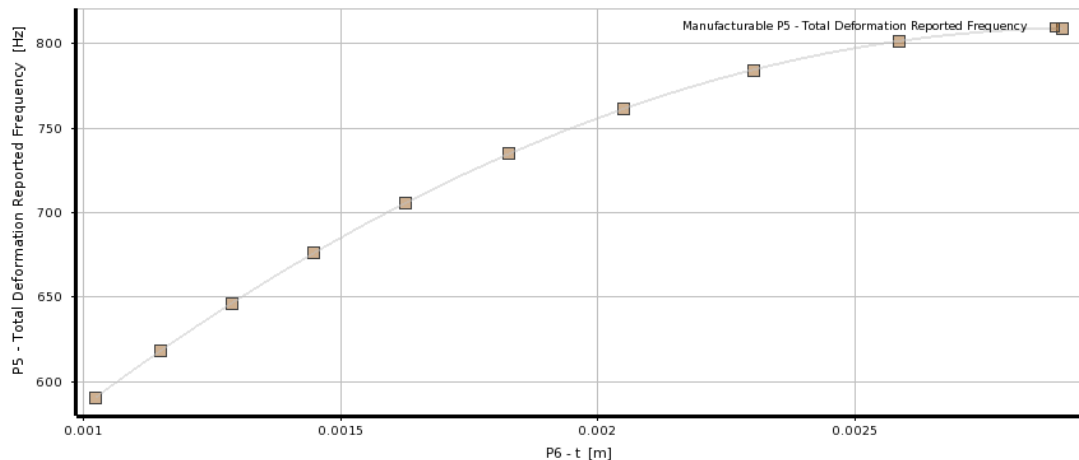


Figure 6.1.2.3. Frequency vs rib thickness.

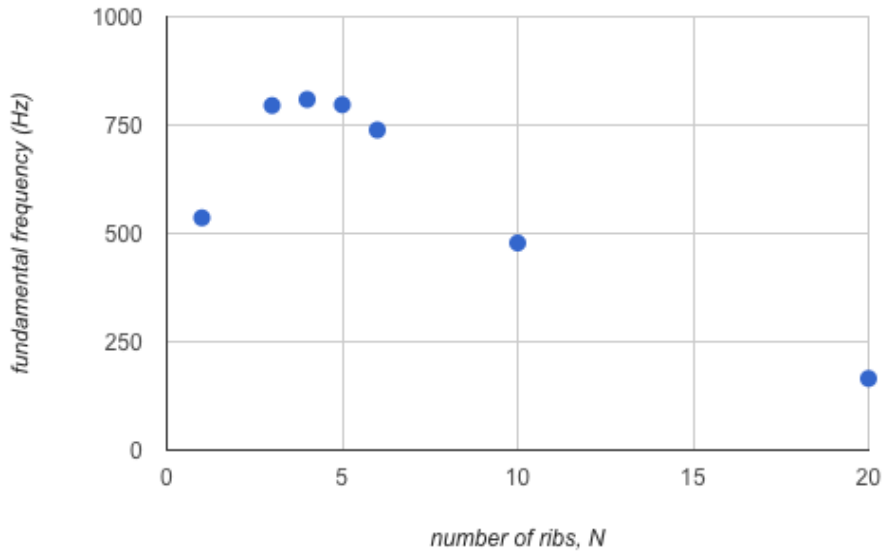
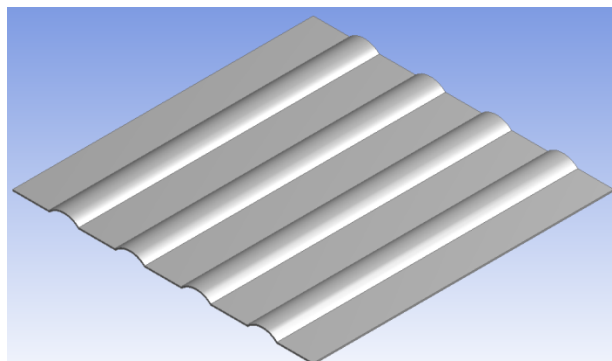


Figure 6.1.2.4. Frequency vs number of ribs.

6.1.3 Optimized Design

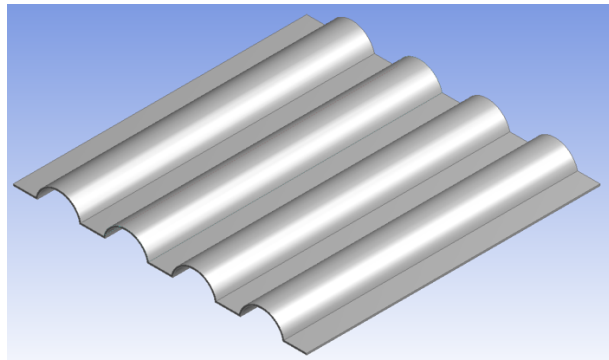
After optimization, the fundamental natural frequency is increased by 176%. Figure 6.1.3.1 and Table 6.1.3.1 compare the initial and optimized designs. The predicted value from the response surface is an accurate approximation of the true value, verified through an additional simulation.



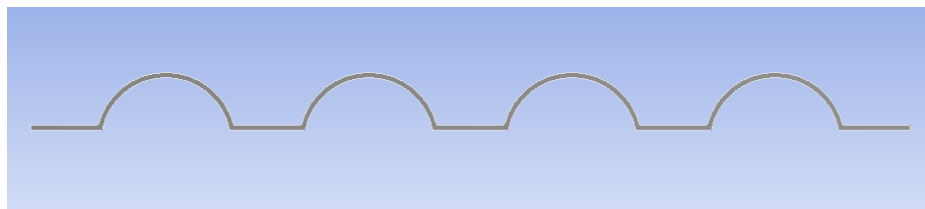
(a) Isometric view of initial design



(b) Cross-sectional view of initial design



(c) Isometric view of optimized design



(d) Cross-sectional view of optimized design

Figure 6.1.3.1. Comparison of initial and optimized panels.

Table 6.1.3.1. Comparison of initial and optimized panels.

Parameter	Initial Design	Optimized Design	
w (mm)	50	77.177	
h (mm)	10	30 (active)	
t (mm)	2.5	2.906 (active)	
N	4	4	
<i>Output</i>	<i>Initial Value</i>	<i>Optimized Value</i>	<i>Simulated Value</i>
Frequency (Hz)	293.63	809.17	809.31

6.1.4 Response Surface, Sensitivity, and Convergence

The MISQP optimization utilizes the response surface created from the design points. Figure 6.1.4.1 below shows that the sample space covers a wide range of objective function values. Design points 1 through 15 were created automatically using a Latin Hypercube sampling method, while the rest were added iteratively to increase the accuracy of the response surface near the optimized region. This corroborates the reliability of the response surface. (Since a Kriging method was used for the response surface, the surface passes through every design point.

Therefore, coefficient of determination is not useful. It is always a perfect 1.0.) Figure 6.1.4.2 shows the response surface itself with regards to two different pairs of variables.

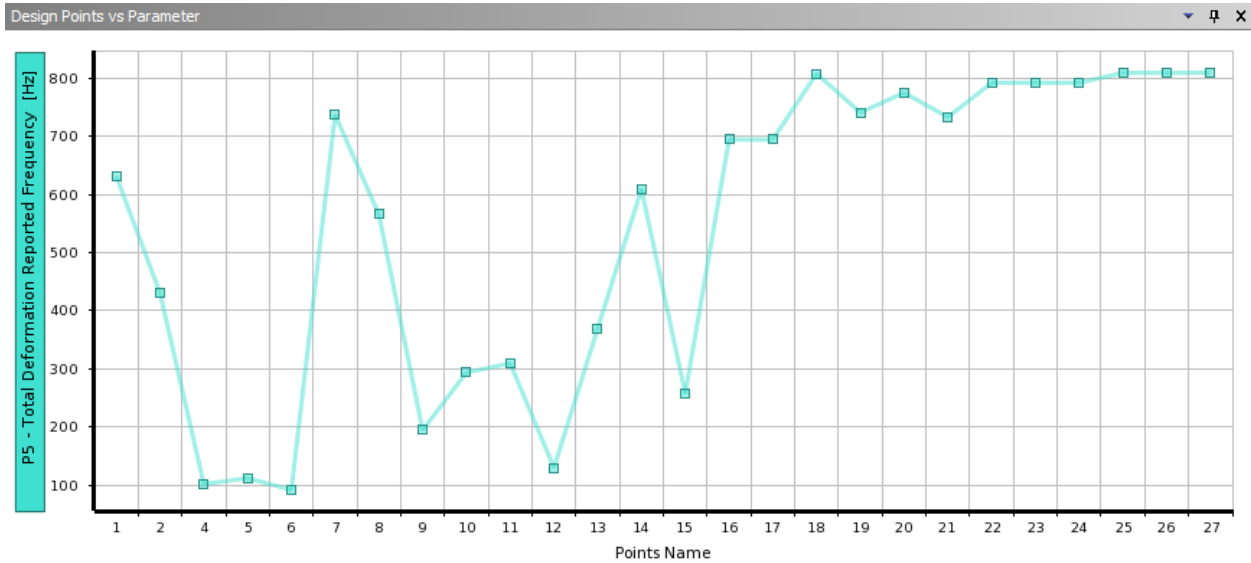


Figure 6.1.4.1. Objective function vs design point number.

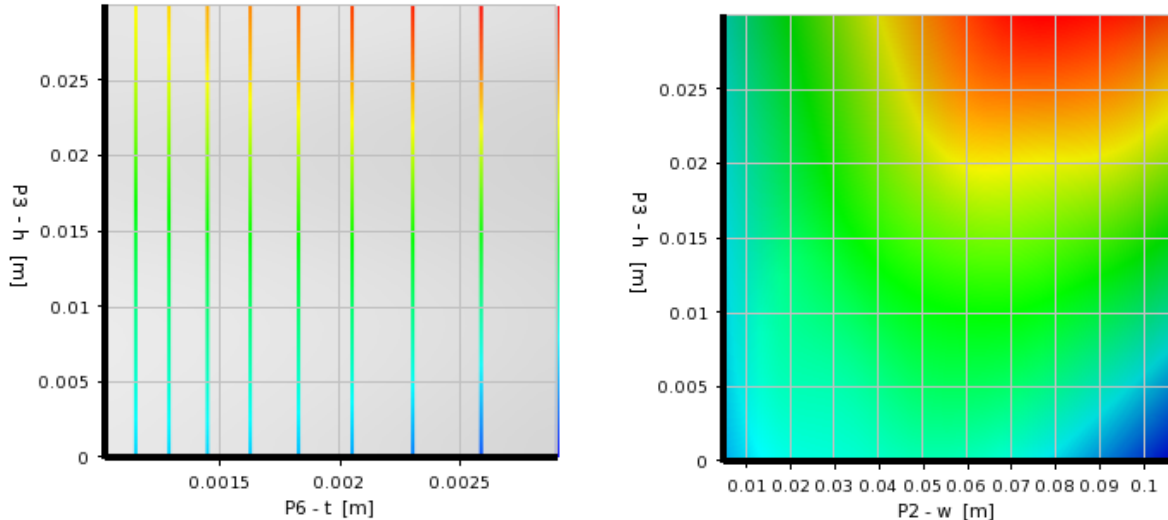


Figure 6.1.4.2. Response surface.

This response surface supports the observation that the height and thickness of the ribs maximize the objective function at boundary values, while width maximizes the objective function at a non-boundary value. Hence, constraints are active for h and t , but not for w .

Accordingly, a plot of the local sensitivity of h , t , and w shows that the frequency could be further maximized if the constraints for h and t were relaxed. However, it should be noted that the sensitivity curve for t is nearly flat at the solution, meaning there would be very small return for relaxing that constraint. Since the optimal value of w does not lie on a constraint, no improvement would come from relaxing its constraint.

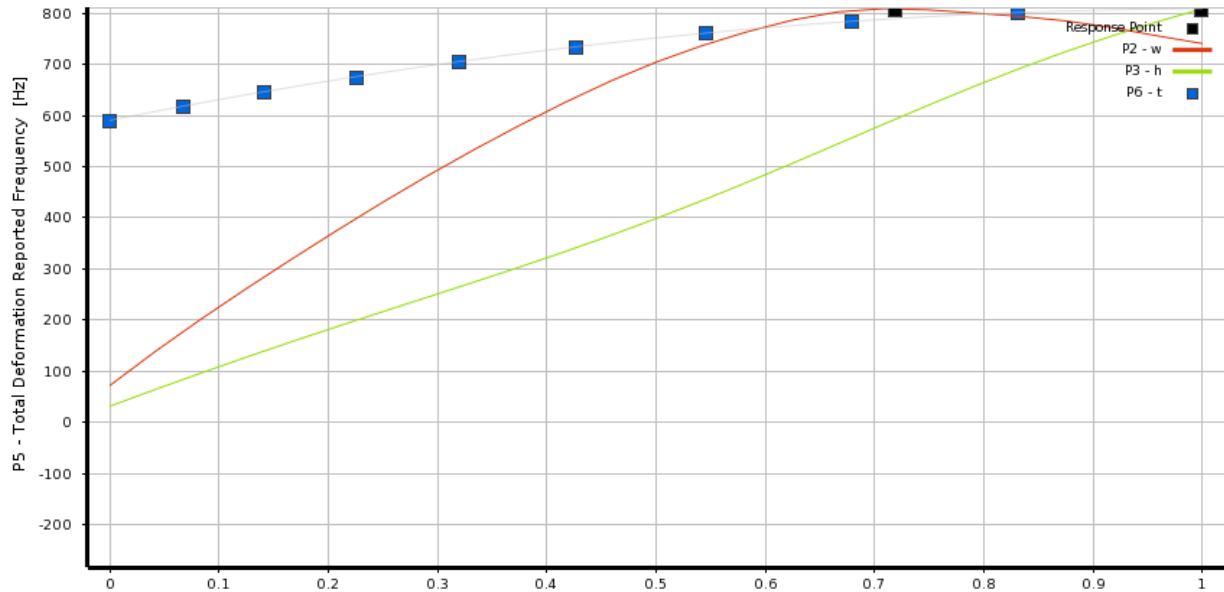


Figure 6.1.4.3. Local sensitivity plot.

Note that the response surface and sensitivity curve could not be generated for N because separate optimizations had to be run for each discrete value of N . Instead, Figure 6.1.4.4 plots the objective function versus N , where each point represents the solution from an optimization with that value of N . A binary search method was used to find the optimal number of ribs. As expected, since the optimal number of ribs does not lie on a constraint, there would be no benefit from relaxing this constraint.

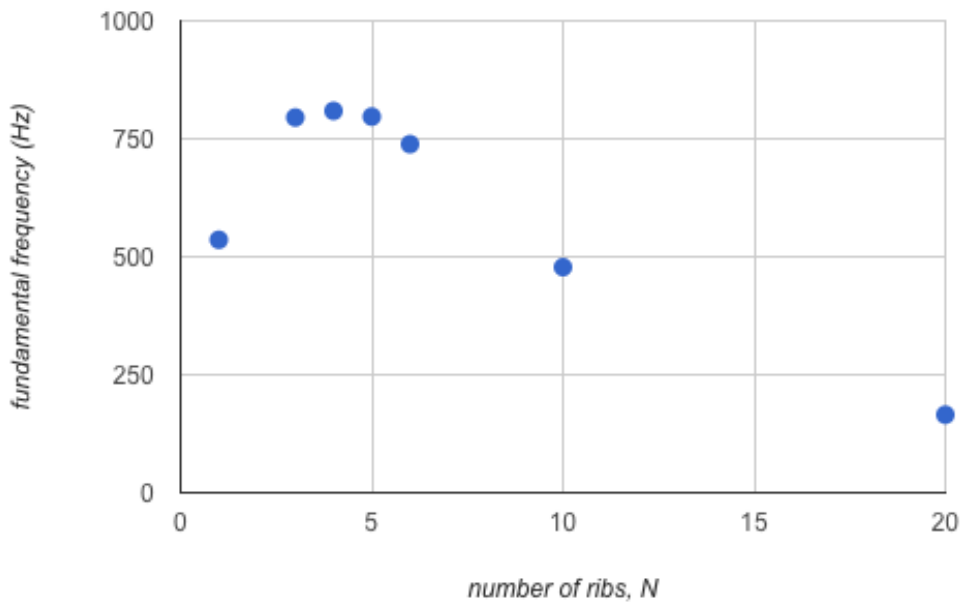


Figure 6.1.4.4. Objective function vs number of ribs.

Finally, a plot of the convergence criteria shows the improvement with each iteration of the MISQP algorithm. The algorithm was started from an initial point near the center of the design space (well away from the solution), in order to demonstrate the robustness of the solver. Figure 6.1.4.6 shows both the starting value and the applied constraints. Note that the domain for t was limited to manufacturable values.

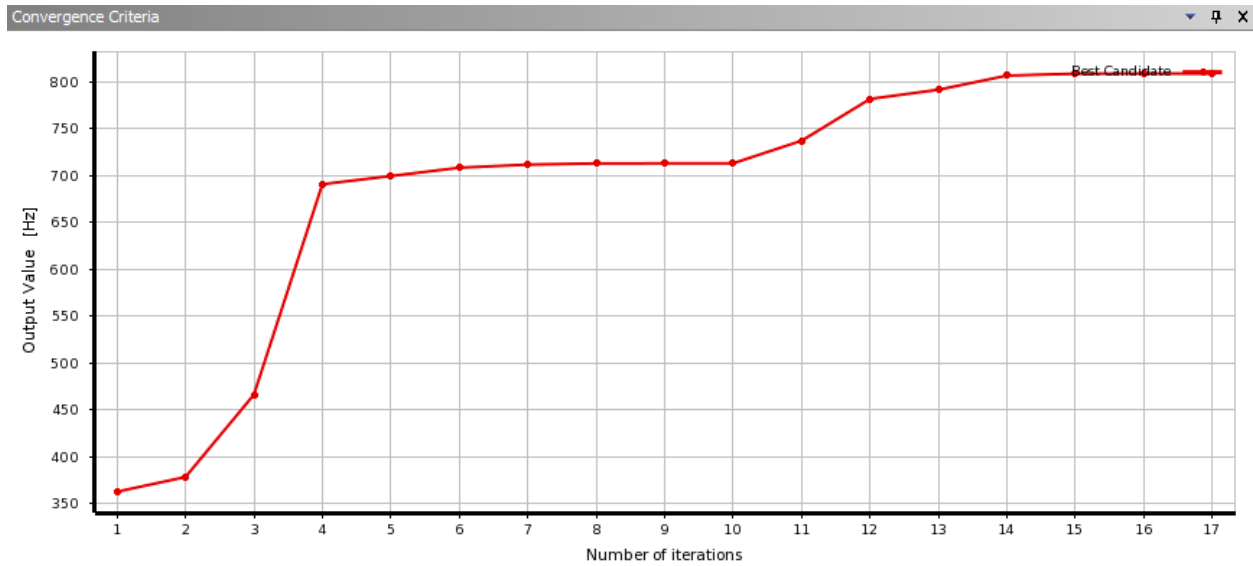


Figure 6.1.4.5. Convergence criteria plot.

Input Parameters				
Name	Lower Bound	Upper Bound	Starting Value	
P2 - w (m)	0.005	0.106	0.05	
P3 - h (m)	0	0.03	0.015	
P6 - t (m)	0.001024	0.002906	0.001628	
Parameter Relationships				
Name	Left Expression	Operator	Right Expression	
P3 <= .5*P2	P3 0.015 [m]	<=	.5*P2 0.025 [m]	

Figure 6.1.4.6. Constraints and start value for response surface optimization.

6.2 Thermal

6.2.1 Initial Design Performance

The thermal capabilities of the original, four ribbed panel had the average temperature of the panel at a relatively high point of 322.03° C. This was worse in analysis than the flat plate due to the non-optimal distribution of surface area that allowed for extra heat transfer to the plate without any substantial increase in heat rejection.

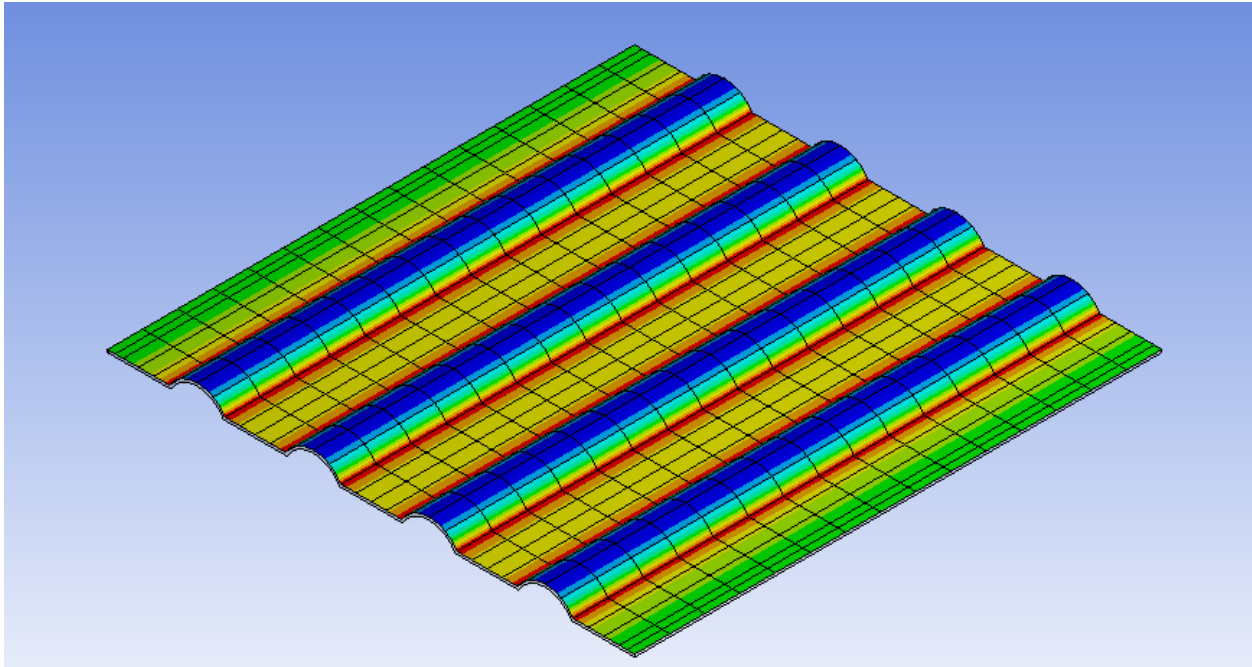


Figure 6.2.1.1. Initial thermal signature.

Jet turbines release a large amount of heat due to their design. They have constant combustion occurring along the length of the body with a high speed turbine in the middle. Pressures and temperatures are extremely high and therefore so is the surrounding areas, especially on aircraft where abundant air cooling is present and there is no need to insulate from the heat.

6.2.2 Parametric Study

The three figures below show the effect of each parameter on the temperature of the plate. These graphs are generated from the response surface based on the design points as well as the optimal values for each rib number tested during the binary search.

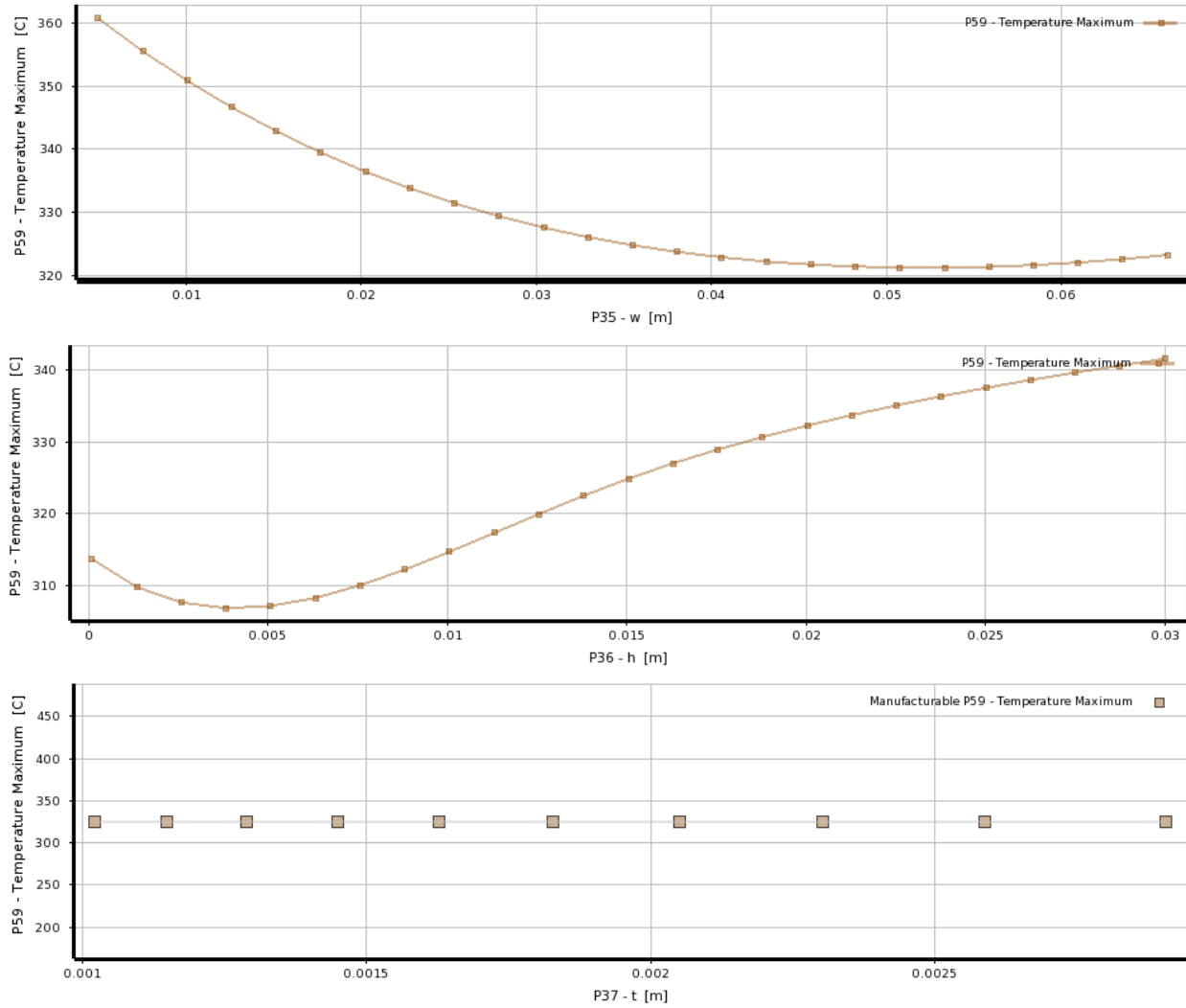


Figure 6.2.2.1. Parametric graphs of temperature versus w, h and t.

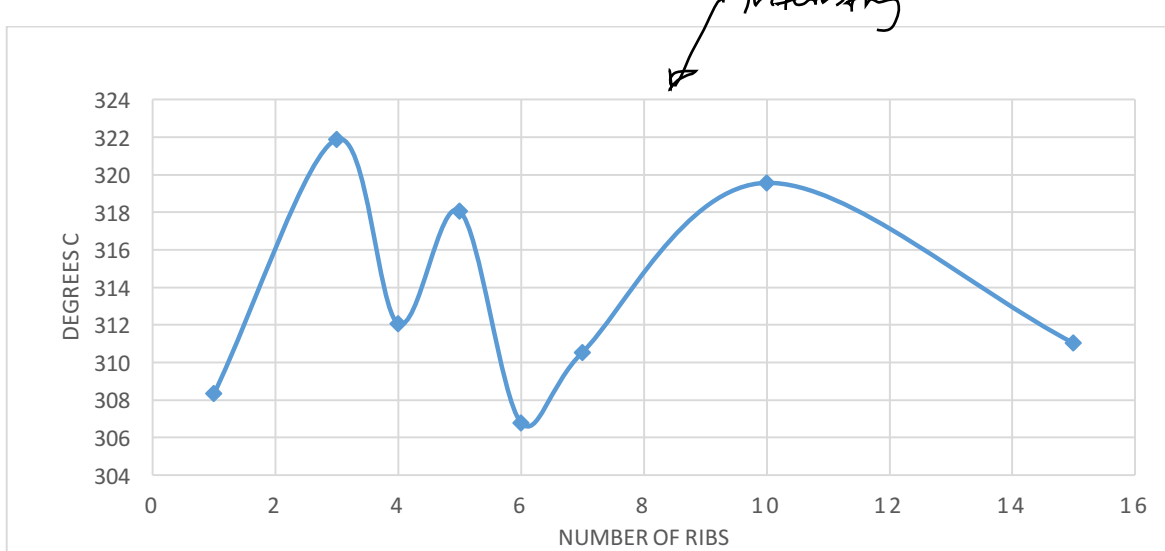


Figure 6.2.2.2. Temperature versus rib number.

The binary search shows where the minimum is due to the finite number of ribs one can have in the plate, however, there is no clear trend. More analysis relating the ribs, their geometry and the relative surface areas with their heat transfer effects is needed to determine if there is larger underlying pattern.

6.2.3 Optimized Design

After a binary search and multiple optimizations, the design shown to be optimal for thermal management was a six ribbed panel with a thickness of 1.29 mm, height of 4.041 mm and width of 2.0152 mm with a final temperature of 306.81°C. This had just under a 5% decrease in average temperature compared to the four ribbed panel. However, the initial temperature of the six ribbed panel was 360.67°C, meaning the decrease to optimal temperature was a 16% improvement. This shows potential for large gains, however, limits such as the height to width ratio limit need to be removed or the material altered. This conclusion is drawn from other optimization tests where larger improvements were quickly seen once that constraint was lifted.

Table 6.2.3.1. Initial and optimized panel values for 6 ribs.

Parameter	Initial Design	Optimized Design	
w (mm)	5	4.0411	
h (mm)	1.5	2.0152	
t (mm)	1.965	1.29	
N	6	6	
Output	Initial Value	Optimized Value	Simulated Value
Temperature (°C)	360.67	306.78	306.81

6.2.4 Response Surface, Sensitivity, and Convergence

A central composite design was used to generate design points for the thermal analysis. This seemed to provide the best coverage of all possibilities as the sampling done with this method produced the most accurate response surfaces for this parameter. The figures below show the parameter graphs and their relations.

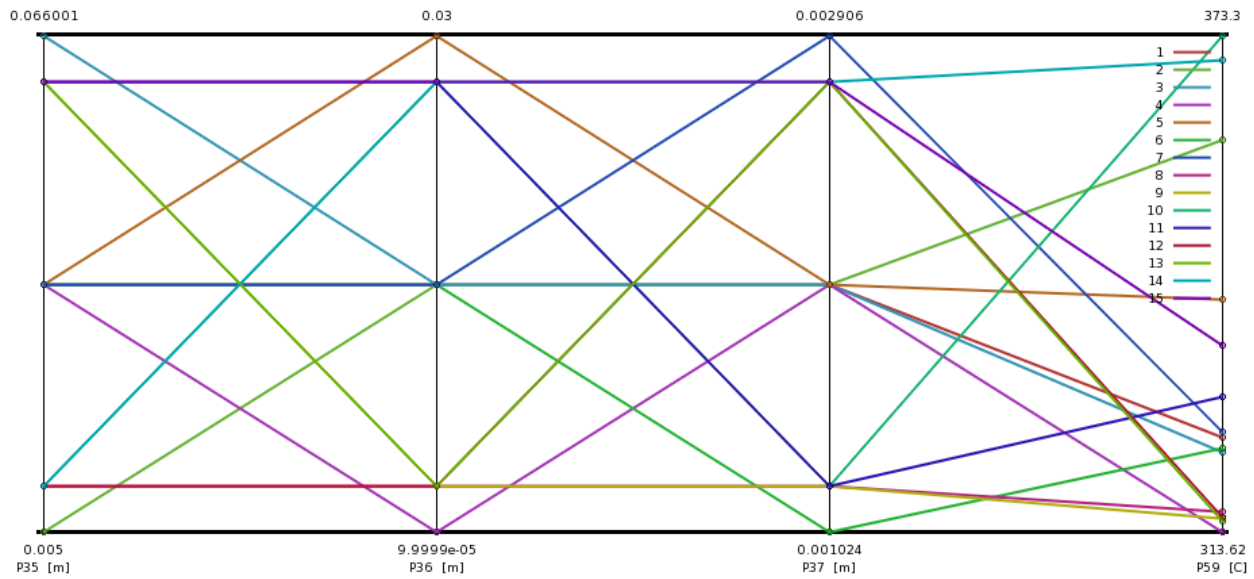


Figure 6.2.4.1. Parameter relations: Parameter Parallel

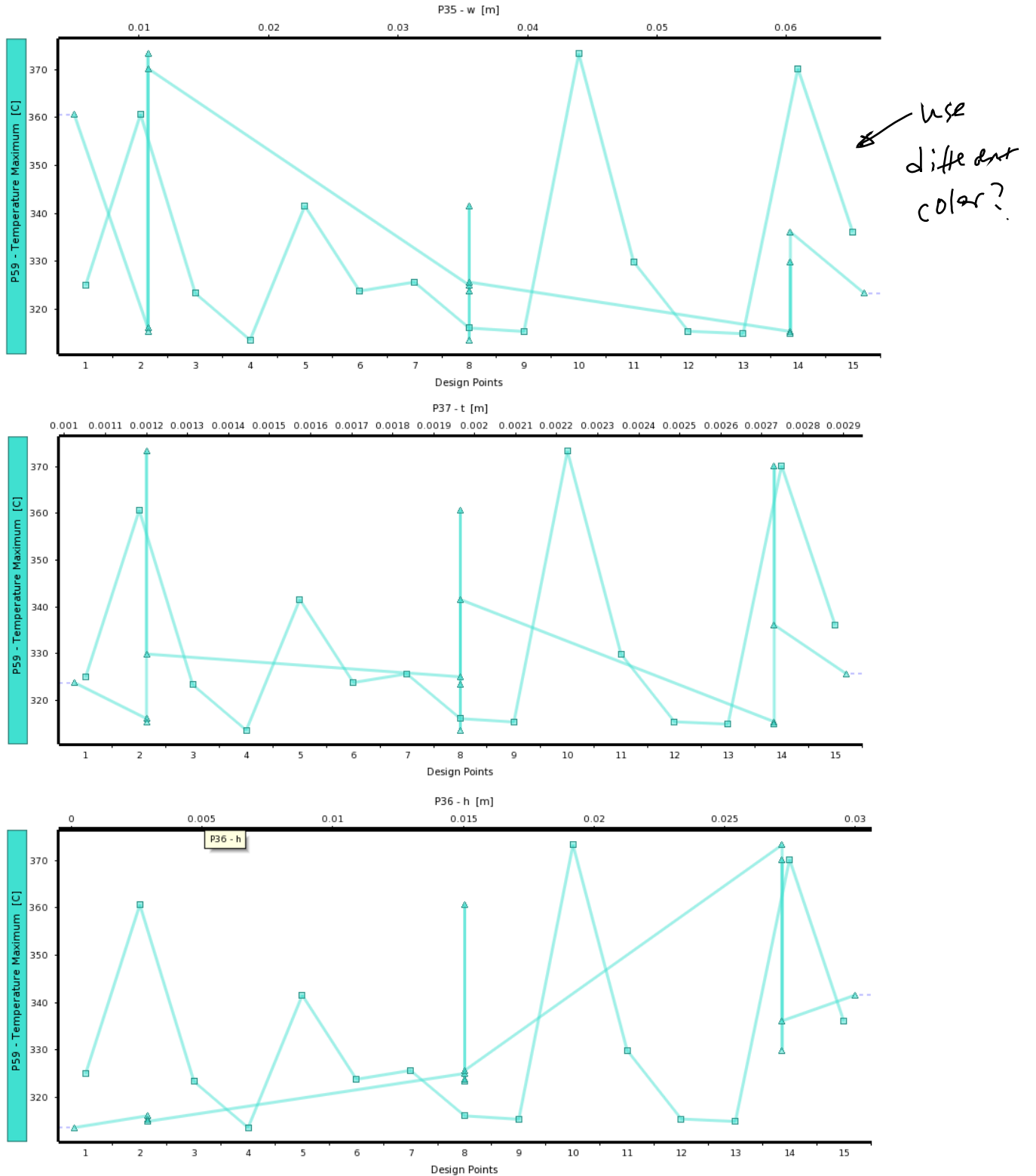


Figure 6.2.4.2. W, t, and h with regards to the design point temperatures found.

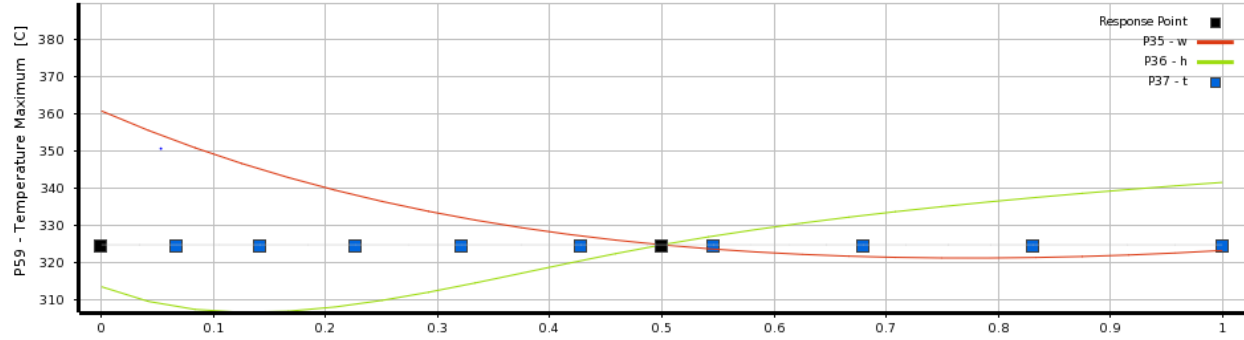


Figure 6.2.4.3. Local sensitivity of the response surface.

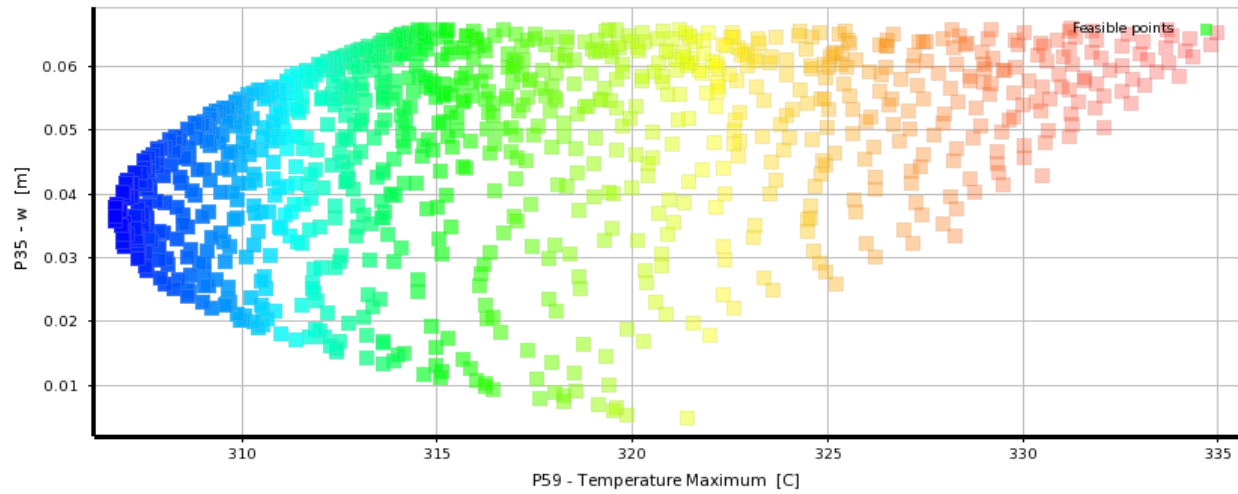


Figure 6.2.4.3. Optimization tradeoff chart.

As mentioned before, the response surface was quite accurate and did not need to converge to come within the needed 1% difference constraint. The minimum value was found to be 306.81°C. Likewise, if the height to width ratio constraint was removed or relaxed slightly, the benefits could have potentially been much better. It is known that the ideal heat sink would have infinitely long fins with as thin geometry as possible to provide the most surface area with the least mass. For this constraint to be relaxed, one would have to look at the forming properties of sheet metal as too long of extrusions will tear the material. Likewise, a more elliptical model with filets to smooth sharp edges would have to be created to ensure the model geometry did not fail or produce unrealistic features. For example, if the height is relatively large while width is small, the solver could interpret this as the majority of the arc sits above the sheet, forming a geometry as shown below. This can be fixed through more constraints being added or other modeling techniques being used, but for the purposes of this research paper will not be explored due to time and processing constraints.

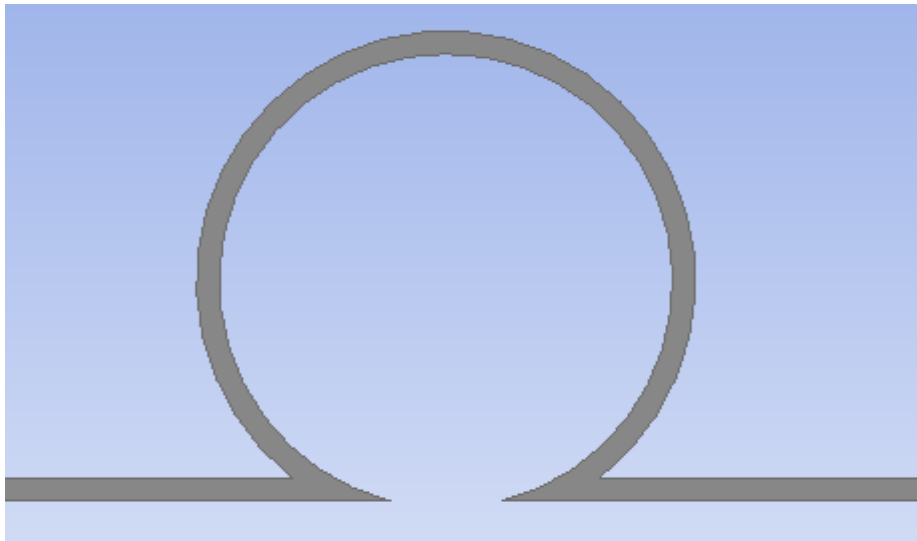


Figure 6.2.4.4. Failed geometry due to relaxed constraints and non-ideal modeling.

6.3 Strength

6.3.1 Initial Design Performance

This pressure created a maximum stress of 38.222 MPa in the first iteration of the panel which had a width of 50 mm, height of 10 mm, thickness of 2.5 mm, and a single rib.

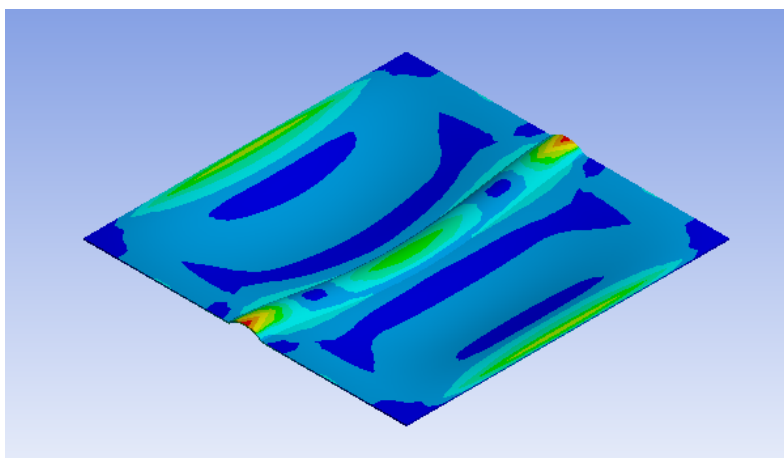


Figure 6.3.1.1. Initial maximum stress results.

Even though our aluminum has a yield strength of 503 MPa, which would give the initial panel a very reasonable design factor of 13.16, there is still room to improve this design factor in order to increase the panel's reliability.

6.3.2 Parametric Study

The first three figures given below display the relationship between each parameter and the maximum stress in the panel with 5 ribs. From the figures it is possible to see that the values for thickness and height mainly increase until they reach the constraints, but the value for width is at an optimum when its value is twice that of the height. The fourth graph displays the binary search for the final parameter, the number of ribs, which was found to be 5. This binary search was necessary because ANSYS couldn't generate the ribs on its own, and so multiple models had to be created in order to optimize this parameter.

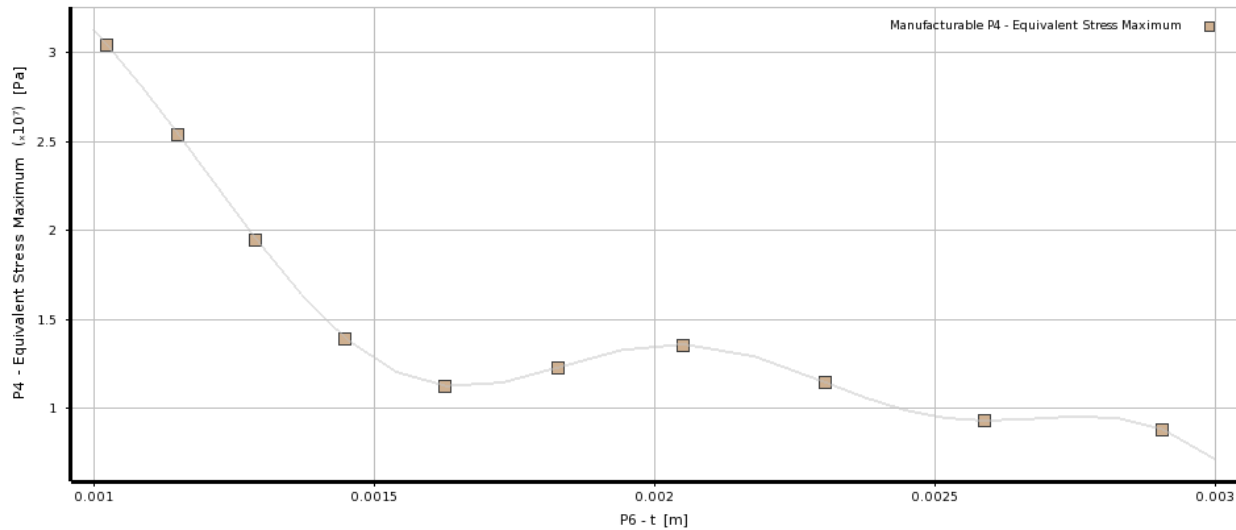


Figure 6.3.2.1. Maximum stress vs rib thickness.

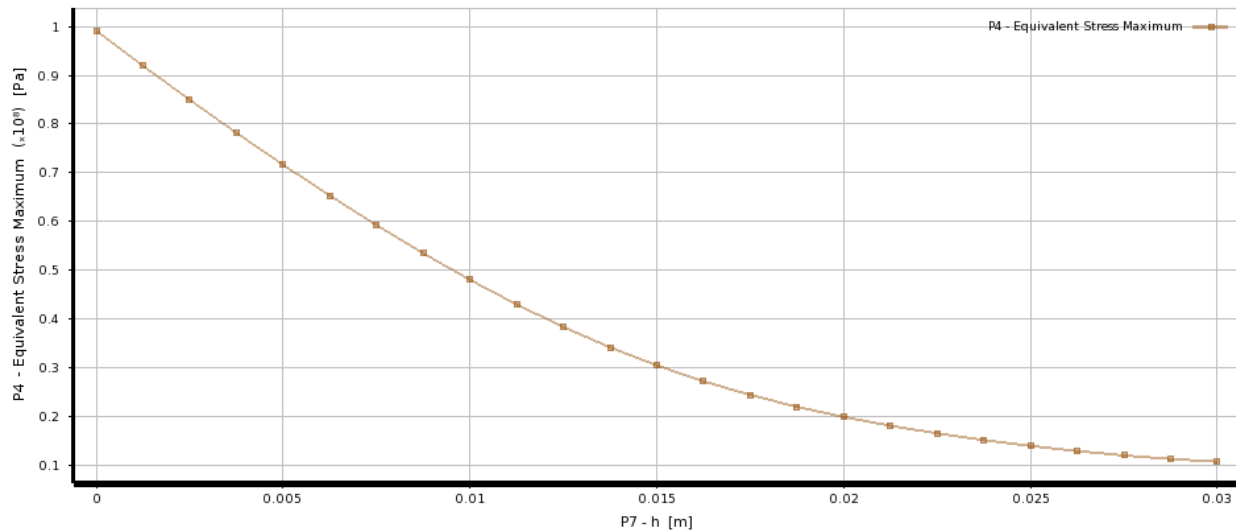


Figure 6.3.2.2. Maximum stress vs rib height.

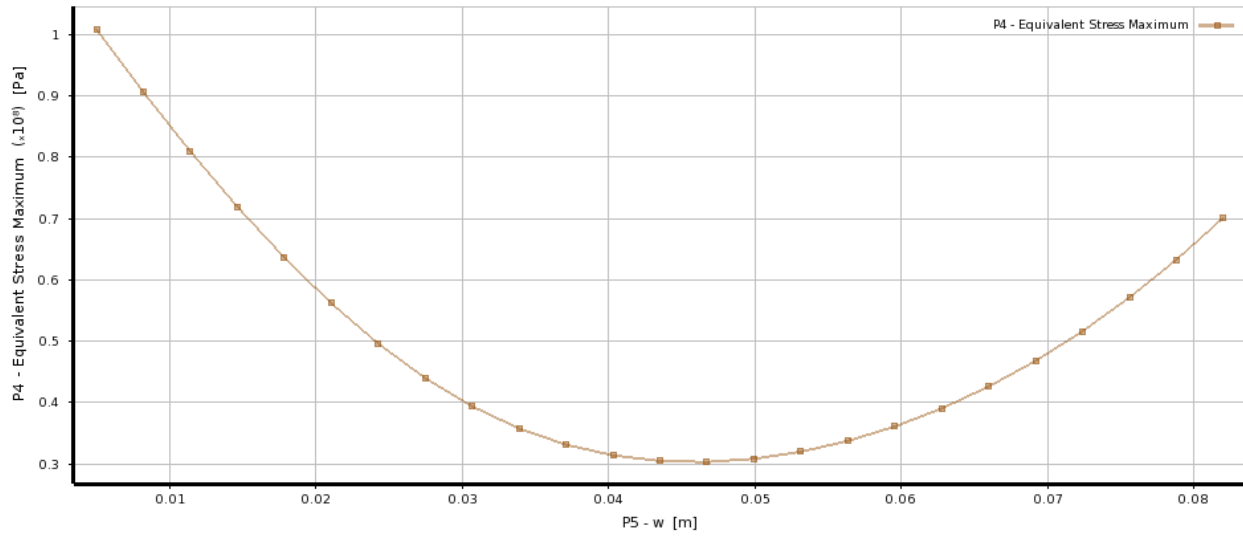


Figure 6.3.2.3. Maximum stress vs rib width.

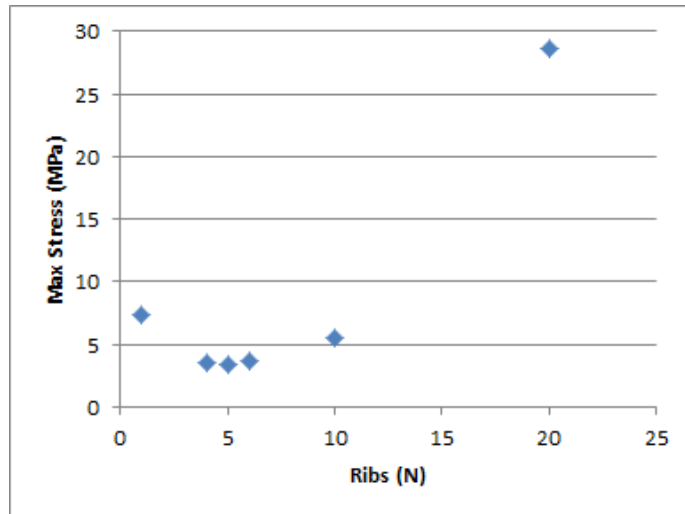


Figure 6.3.2.4. Maximum stress vs number of ribs.

6.3.3 Optimized Design

After doing a binary search to find the optimum number of ribs, the final optimum design was found to be a width of 60 mm, height of 30 mm, thickness of 2.906 mm, and 5 ribs. As seen in Table 6.3.3.1, the final maximum stress from the response surface was 3.3899 MPa which is an improvement of 1127.5% from the initial value. The final maximum stress value was also verified with the results shown in Figure 6.3.3.2.

Table 6.3.3.1. Comparison of initial and optimized panels.

Parameter	Initial Design	Optimized Design
w (mm)	50	60
h (mm)	10	30
t (mm)	2.5	2.906
N	1	5
Output	Initial Value	Optimized Value
Max Stress (Pa)	38.222 MPa	3.3899 MPa

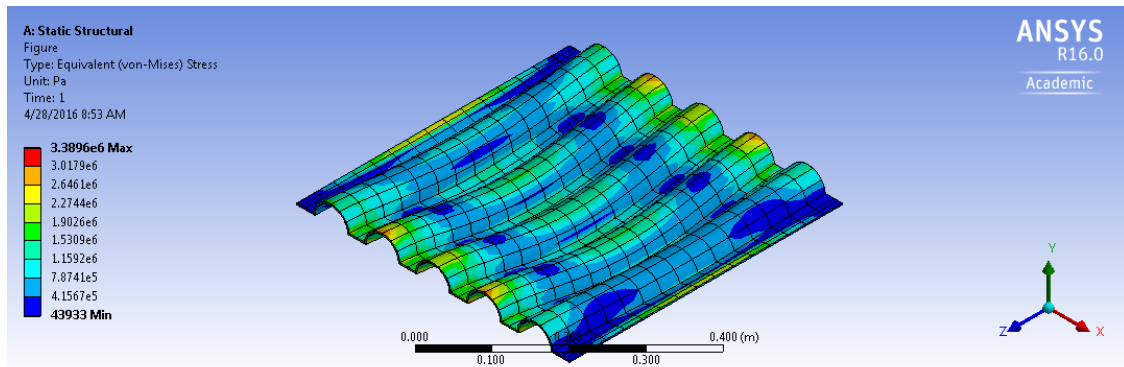


Figure 6.3.3.2. Simulated maximum stress design point.

6.3.4 Response Surface, Sensitivity, and Convergence

Shown below in Figures 6.3.4.1 are two graphs of the response surface that show the relationship between the height, thickness, and maximum stress as well as the height, width, and maximum stress. The graph of height and thickness from the response surface backs up the assertion that as both of these values increase the maximum stress decreases. The second graph is more interesting because the width doesn't continually decrease the maximum stress as it increases. It is an optimum when it is double the height. We know that a sphere is the best pressure vessel, and so intuitively it makes sense that a semicircle (which is created when the width is double our height) is the best design for our rib.

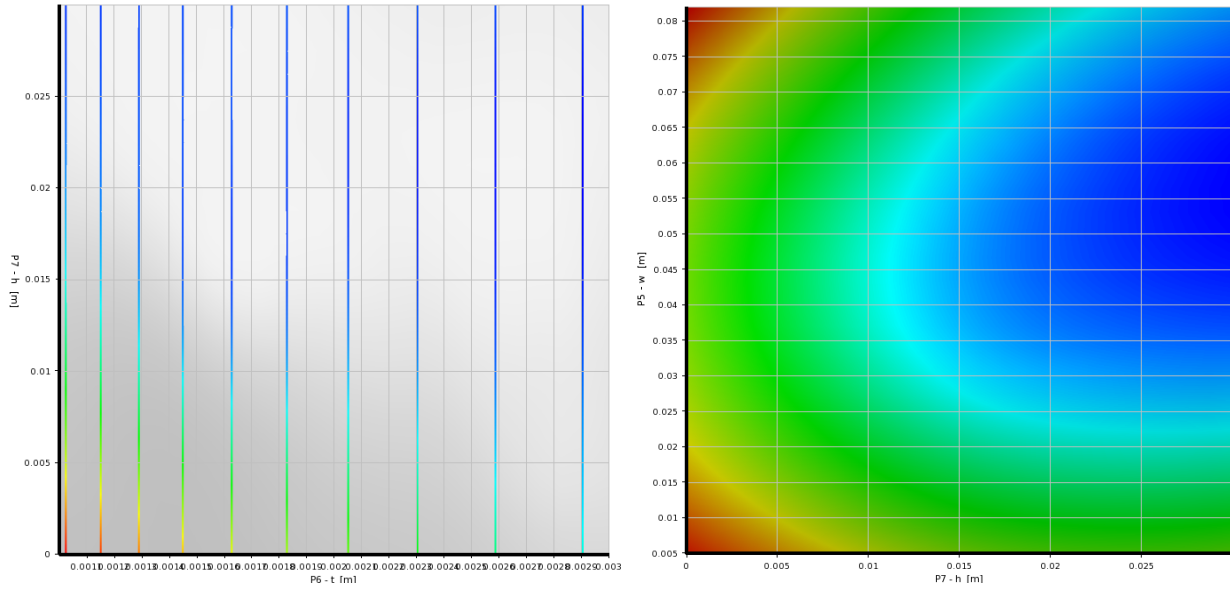


Figure 6.3.4.1. Response surface.

The graph of sensitivity which is shown below in Figure 6.3.4.2 shows that the height and thickness could be further optimized if the constraints were relaxed. However, the slope of thickness seems to indicate that the improvement from relaxing this constraint would not be very impactful.

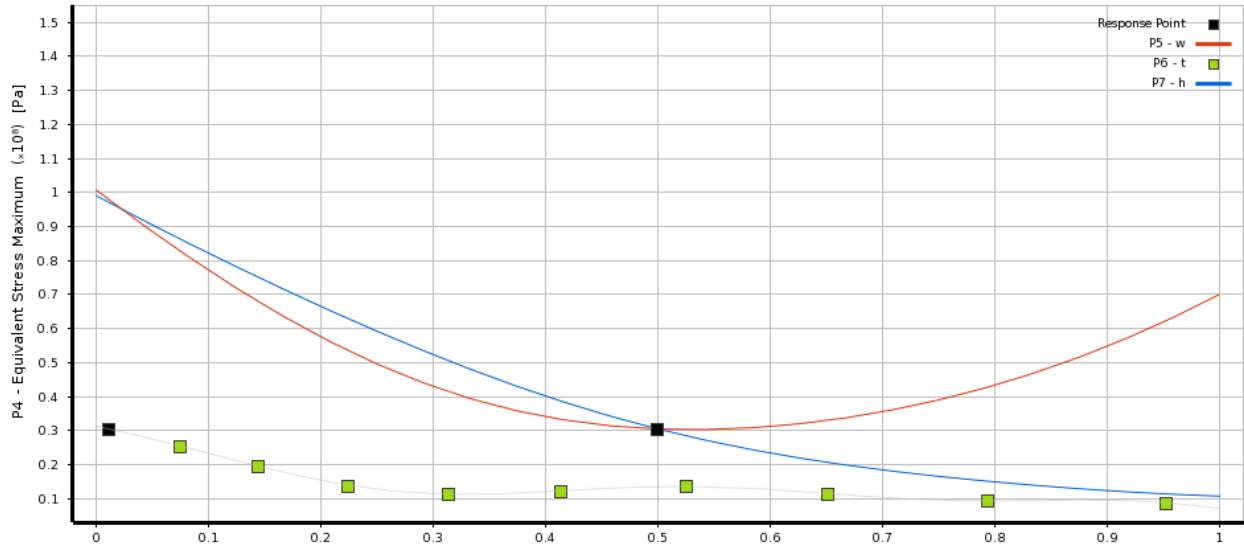


Figure 6.3.4.2. Local sensitivity plot.

Figure 6.3.4.3 below shows the convergence of the MISQP algorithm as it improves with each iteration. The starting point for this optimization was 0.0435 m for the width, 0.002906 m for the thickness, and 0.015 m for the height.

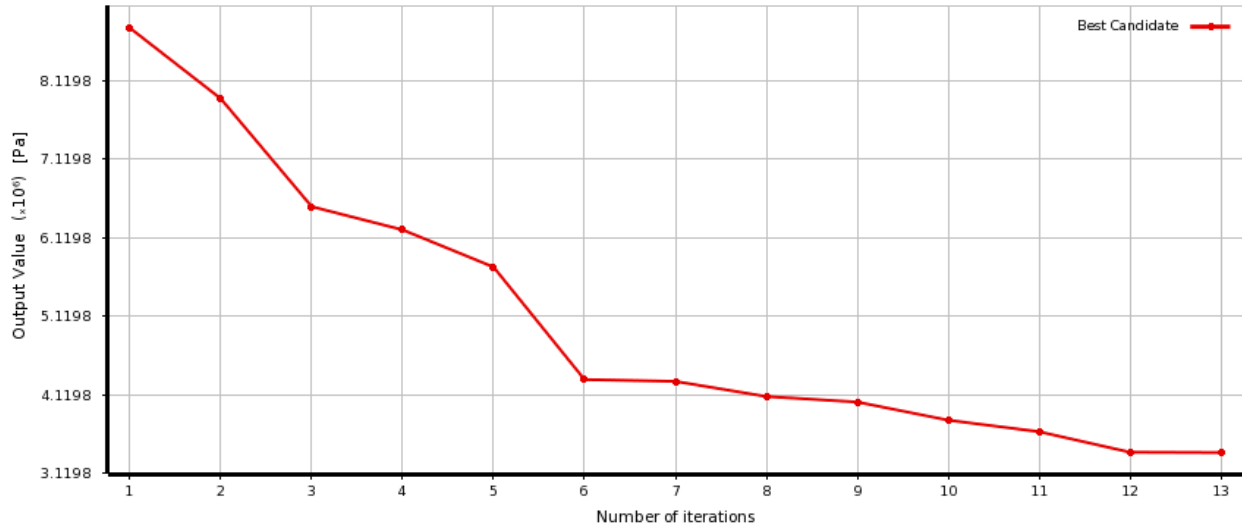
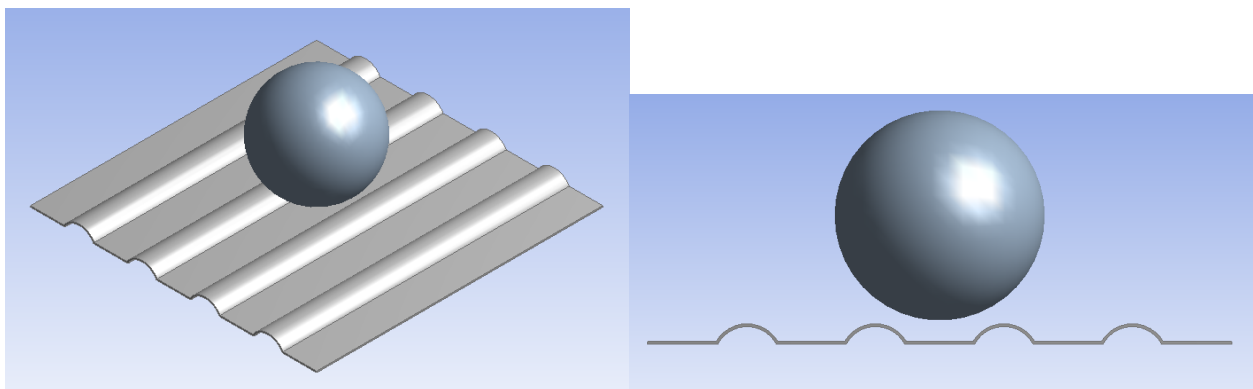


Figure 6.3.4.3. Convergence criteria plot.

6.4 Impact Strength

6.4.1 Initial Design Performance

The initial design for impact analysis can be seen in Figure 6.4.1.1 and design parameters and objective function output are tabulated in Table 6.4.1.1.



(a) Isometric view of initial design

(b) Cross-sectional view of initial design

Figure 6.4.1.1. Initial design for impact analysis.

Table 6.4.1.1. Initial design parameters.

Variable/Objective	Impact Analysis
h (mm)	15
w (mm)	50
t (mm)	2.5
N (# of ribs)	4
Max Equivalent Stress (GPa)	3.5967

The stress map at the time of maximum equivalent stress for the original design is shown in Figure 6.4.1.2.

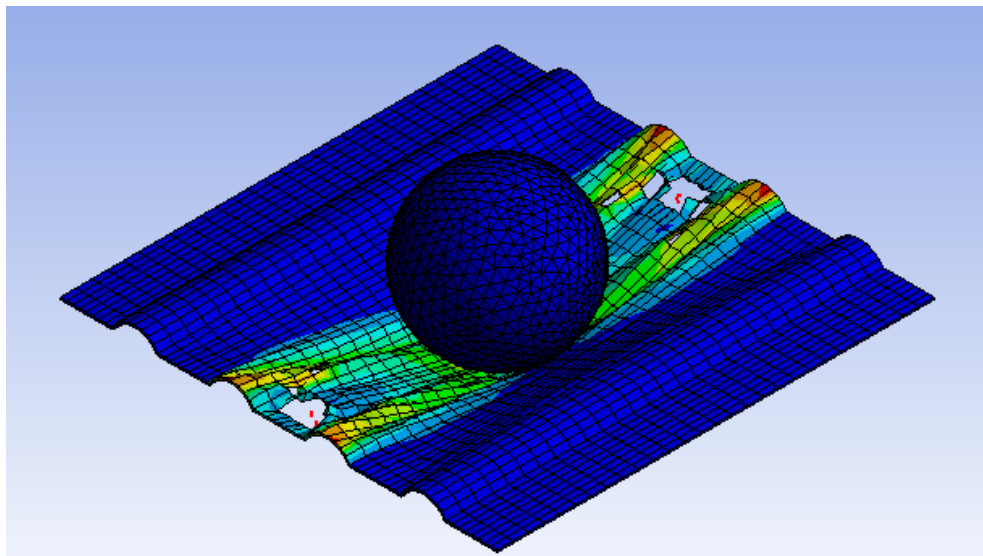


Figure 6.4.1.2. Stress map at time of maximum equivalent stress.

6.4.2 Parametric Study

Figures 6.4.2.1 through 6.4.2.4 show the effect of w , h , t , and N on the maximum equivalent (Von Mises) stress of the panel. The parameters not included in each respective plot are at their optimized values, except for the plot of stress vs N , for which each point is the optimum solution for that number of ribs.

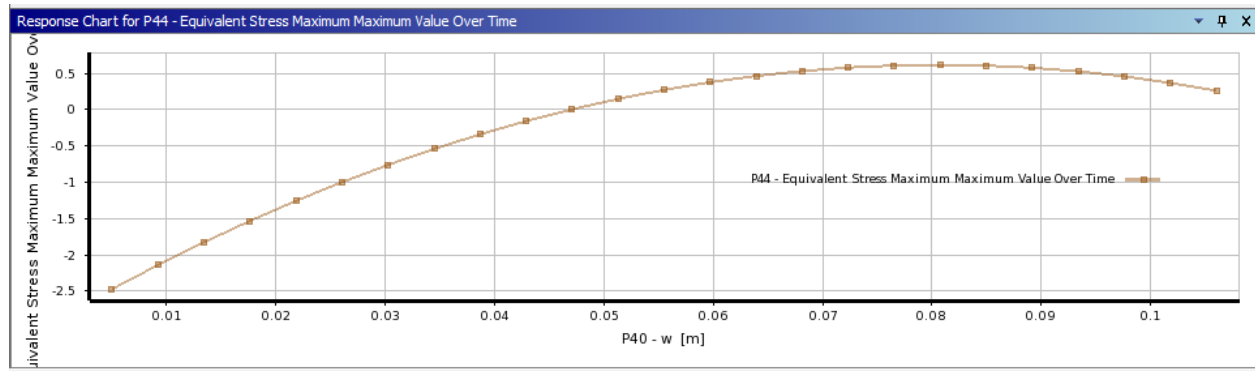


Figure 6.4.2.1. Equivalent stress vs. rib width.

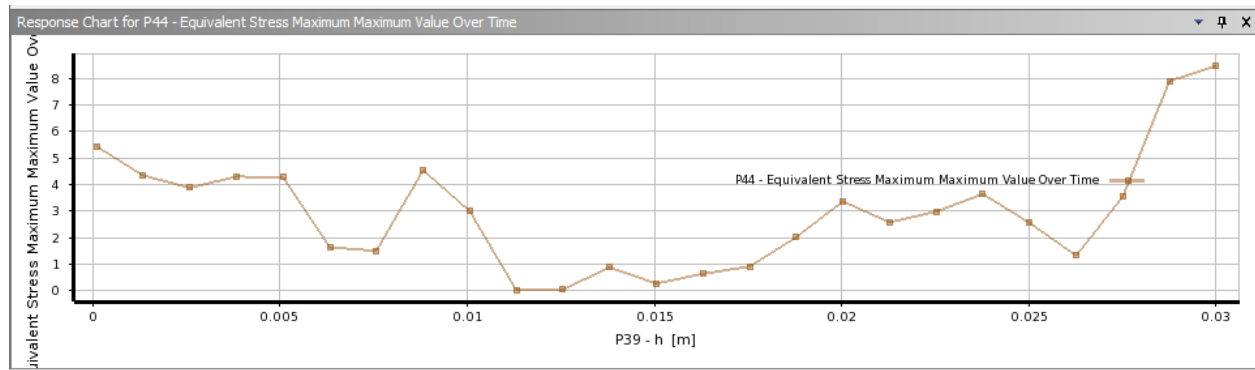


Figure 6.4.2.2. Equivalent stress vs. rib height.

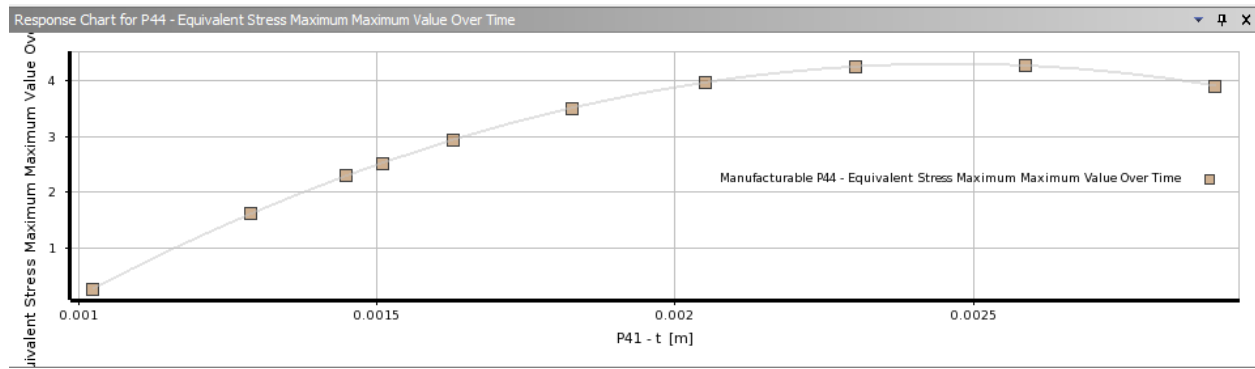


Figure 6.4.2.3. Equivalent stress vs. rib thickness.

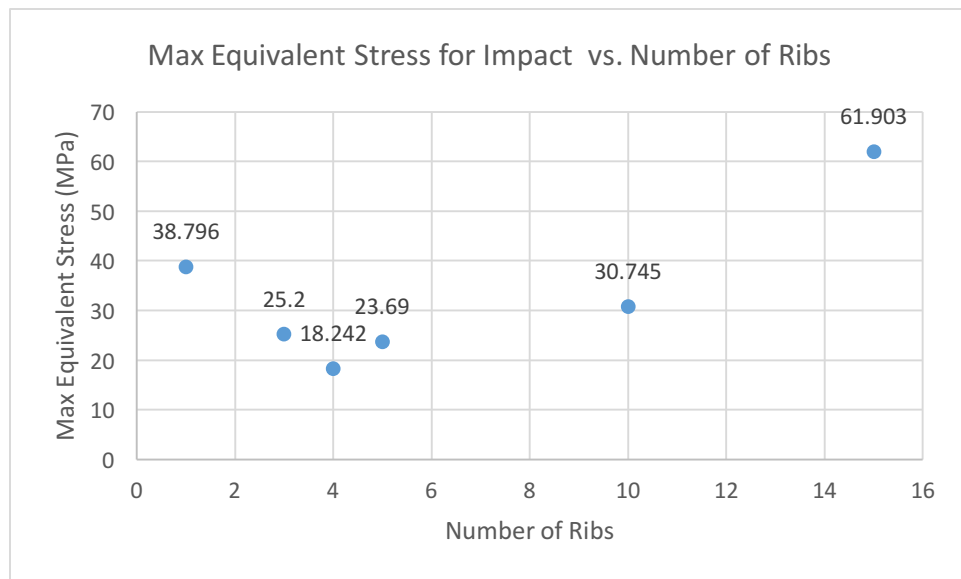


Figure 6.4.2.4. Equivalent stress vs. number of ribs.

Note that a response surface could not be generated for number of ribs because separate optimizations had to be run for each value of N. A binary search method was used to determine the optimal N value and then optimization was performed on the parameters of the rib (h, w, t) for each distinct geometry. As shown by the binary search show in Figure 6.4.2.4, the number of ribs is not an active constraint so there is no benefit from relaxing this constraint.

6.4.3 Optimized Design

After optimization, the maximum equivalent stress was decreased by 6.8228%. Figure 6.4.3.1 shows the new optimal design.

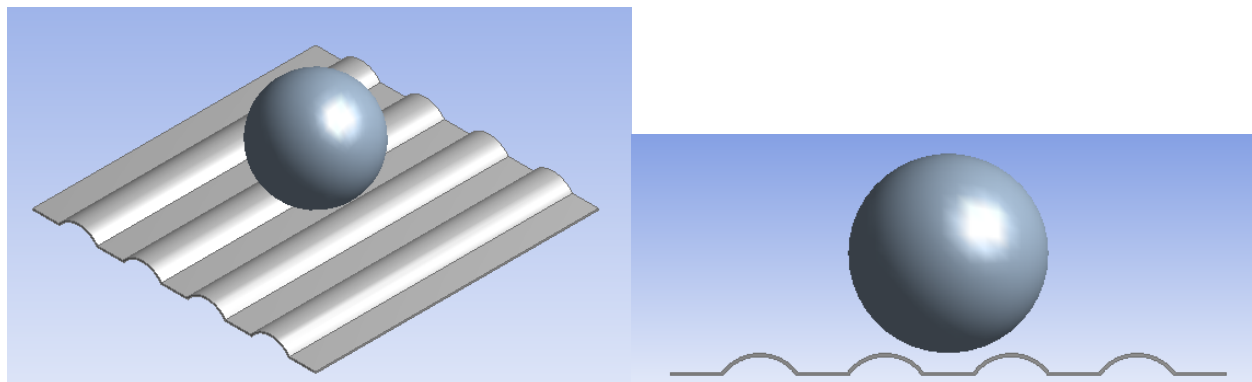


Figure 6.4.3.1. Optimized design for impact analysis.

The final parameters, results and verification of results by re-evaluation of the objective function from the predicted model are displayed in Table 6.4.3.1 below.

Table 6.4.3.1. Optimized results.

Parameter	Initial Design	Optimized Design	
w (mm)	50	65.813	
h (mm)	15	17.129	
t (mm)	2.5	2.906	
N	4	4	
<i>Output</i>	<i>Initial Value</i>	<i>Optimized Value</i>	<i>Simulated Value</i>
Equivalent Stress (GPa)	3.5967	3.3594	3.3846

This is a 632% improvement upon the flat plate design evaluated to experience a maximum stress of 24.6 GPa. Though these values are far beyond the yield stress of the material, the trend in the reduction of stress is still seen as valid.

The stress map at the time of maximum equivalent stress for the optimal design is shown in Figure 6.4.3.2.

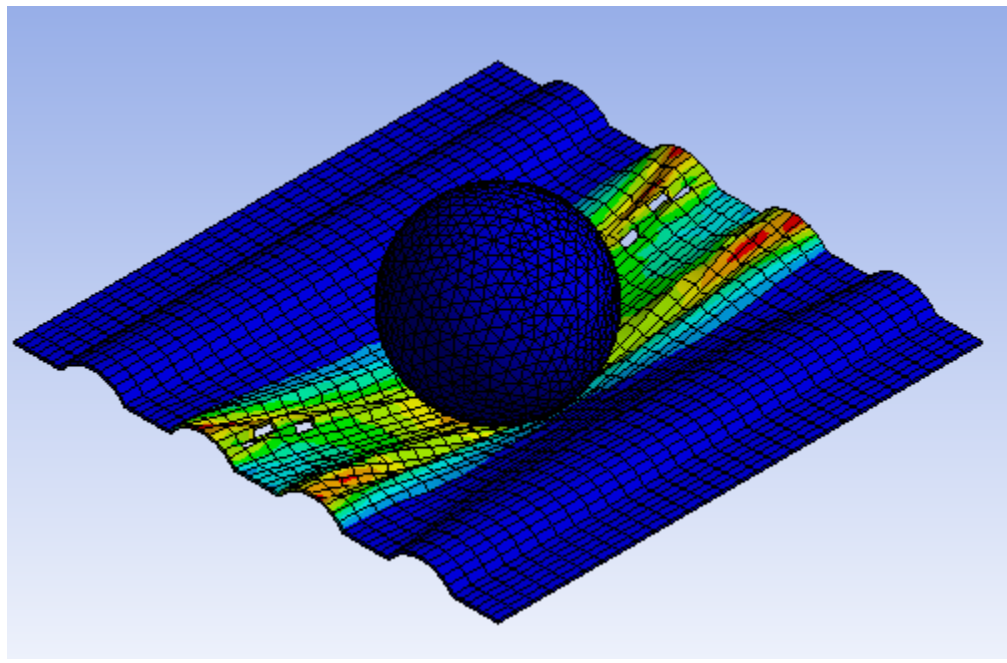


Figure 6.4.3.2. Stress map at time of maximum equivalent stress.

6.4.4 Response Surface, Sensitivity, and Convergence

The MISQP optimization was used for a response surface created from the design points, the first 25 of which were automatically generated by a Latin Hypercube sampling method. All design points after the first 25 were iteratively generated based on the previous iteration until the verified value using the determined optimized parameters was within 1% of the optimized model value. A Kriging method eliminated the usefulness of the coefficient of determination as this method dictates that the surface passes through every design point. Figure 6.4.4.1 shows the progression of the objective function through each iteration of the design.

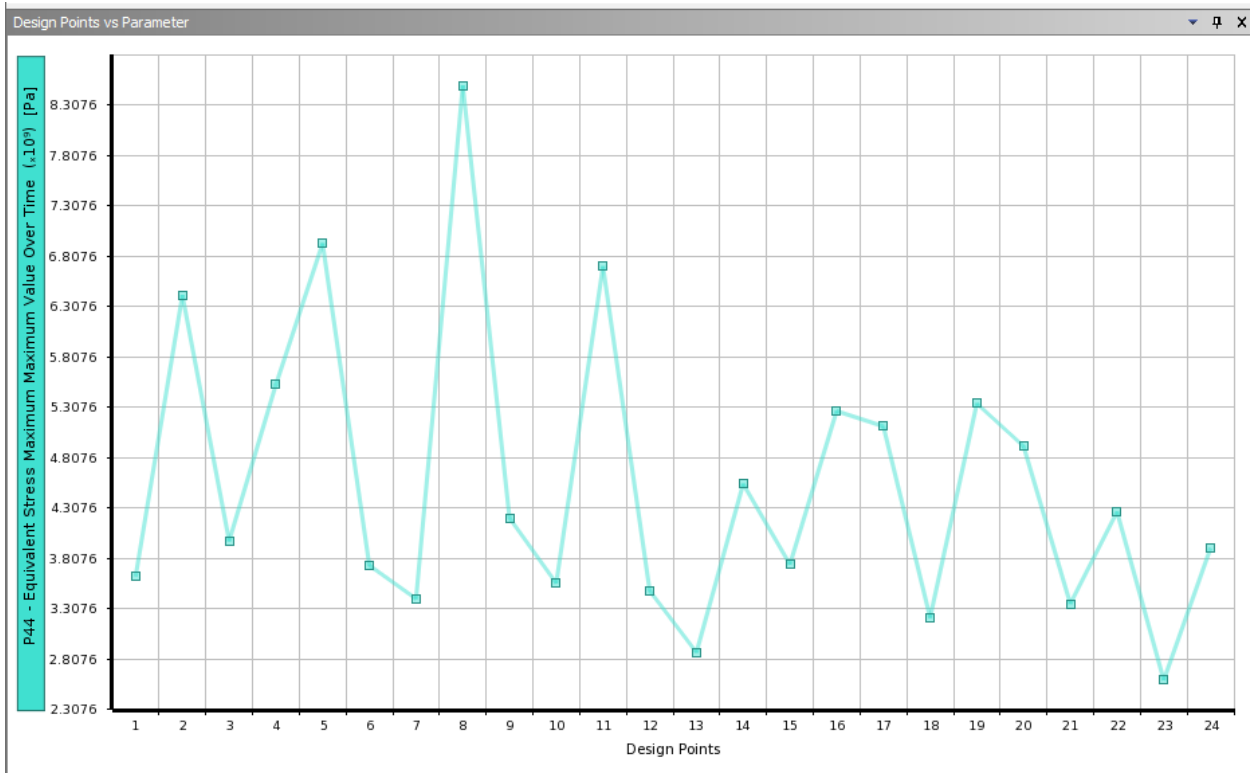
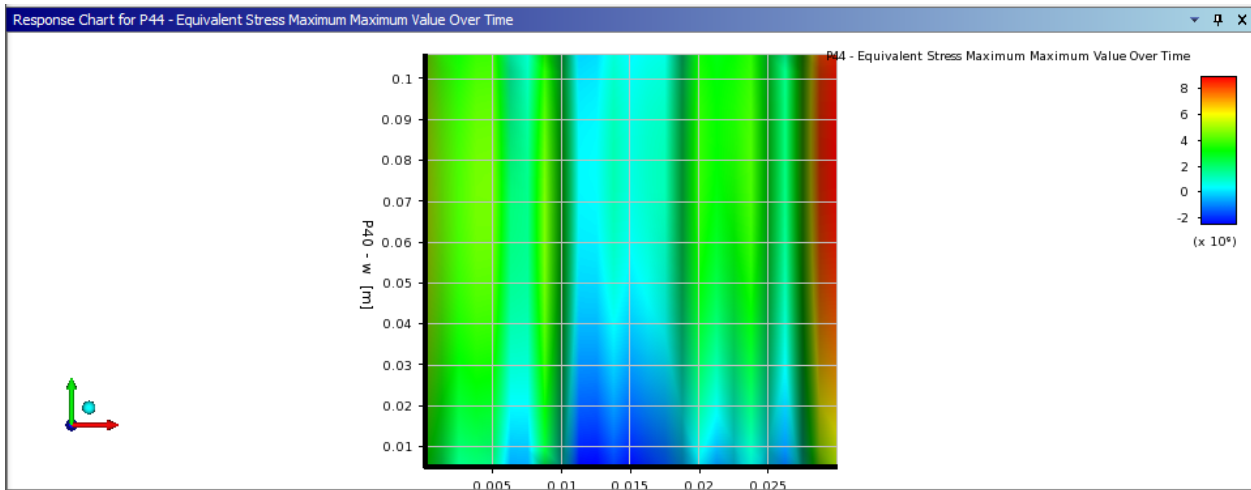
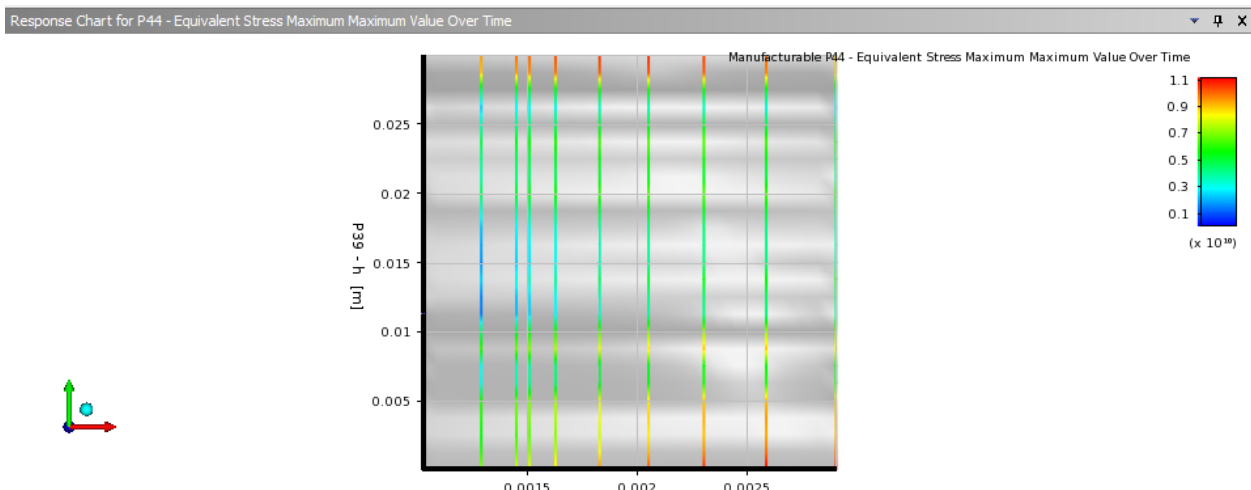


Figure 6.4.4.1. Objective function vs. design point number.

Figure 6.4.4.2 shows the response surface with respect to two pairs of variables.



(a) Response surface w vs. h .



(b) Response surface h vs. t .

Figure 6.4.4.2. Response surfaces.

The response surface shows that thickness maximizes the objective function at the boundary values, while width and height maximize it at non-boundary values. This means that thickness is the only active constraint.

The sensitivity curves of the variables at the solution, shown in Figure 6.4.4.3 below, demonstrate the activity of the constraints. They also indicate the relative “return” to be had from relaxing the constraints on each variable. Variables that do not lie on active constraints have no return for relaxing the corresponding constraint.

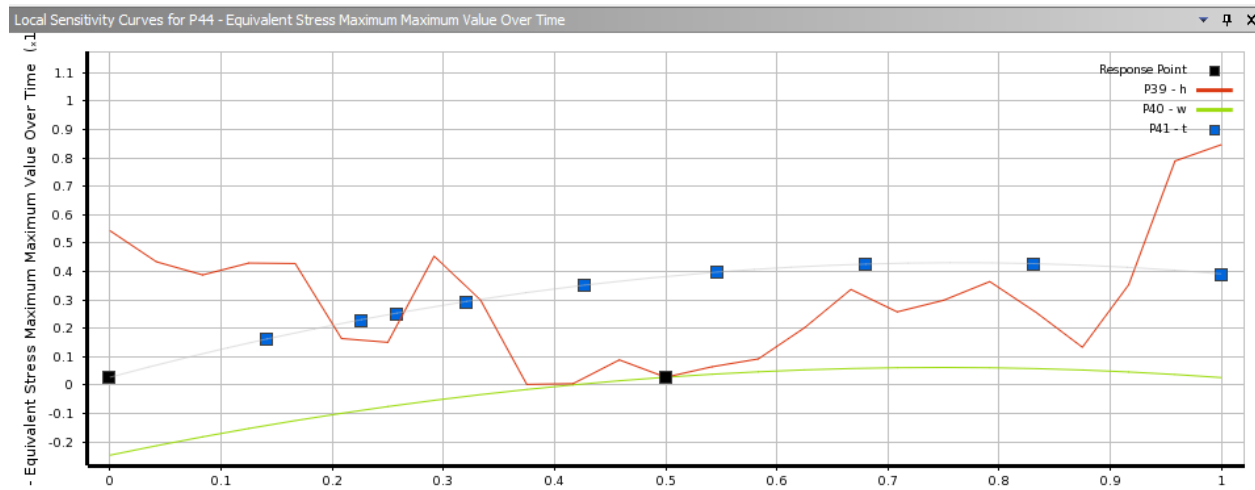


Figure 6.4.4.3. Local sensitivity plot.

Lastly, a convergence plot shows the improvement of the objective function of each iteration for minimizing the maximum equivalent stress.

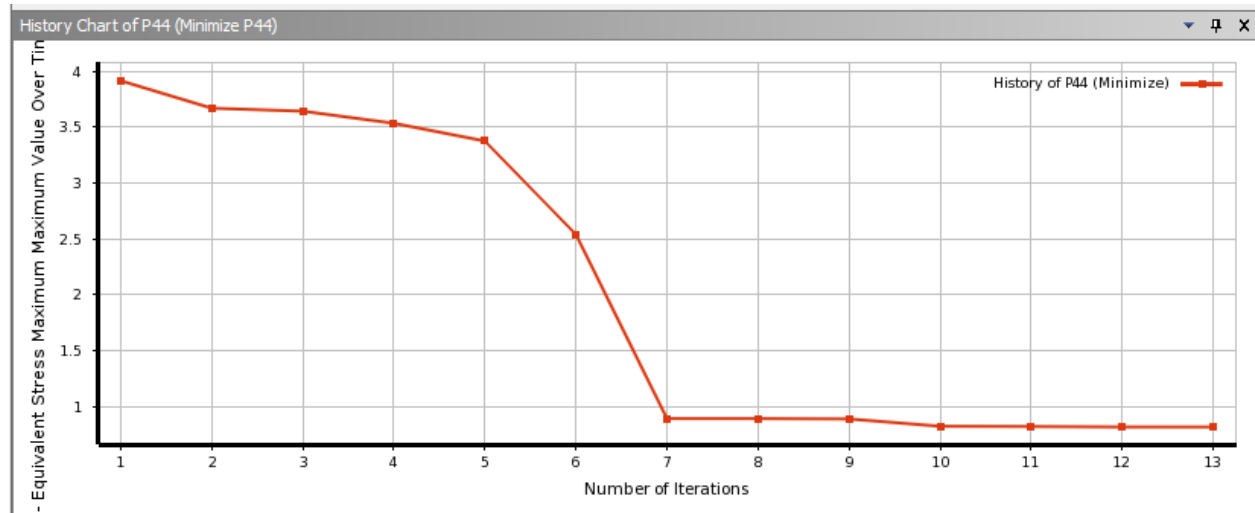


Figure 6.4.4.5. Convergence criteria plot.

Input Parameters			
Name	Lower Bound	Upper Bound	Starting Value
P39 - h (m)	0.0001	0.03	0.01505
P40 - w (m)	0.005	0.106	0.0555
P41 - t (m)	0.001024	0.002906	0.002906
Parameter Relationships			
Name	Left Expression	Operator	Right Expression
P39 <= .5*P40	P39 0.01505 [m]	<=	.5*P40 0.02775 [m]

Figure 6.4.4.6. Constraints and start value for response surface optimization.

7 System Optimization

7.1 Process

System optimization was performed using a response surface optimization with Latin Hypercube Sampling, a Kriging response surface, and a Multi-Objective Genetic Algorithm (MOGA) for optimization on that response surface. This algorithm is ideal for finding pareto-optimal points, which represent the optimal solution for a given balance of the objective functions; that is, a given objective function could not be optimized any further without compromising the optimization of the other objective functions. Separate sampling schemes and optimizations were performed for $N = 4, 5$, and 6 ribs, since these are the three optimal numbers of ribs from the submodel optimization. Using 20 pareto-optimal points from the MOGA optimization for each distinct value of N , linear regression was performed in MATLAB to generate a second-order pareto-optimal surface. The code for this process is shown in the Appendix. A pareto-optimal surface from both constant-bias and linear-bias Kriging methods was also considered, but these methods generated surfaces without meaningful trends.

Originally, this process was attempted with all four submodels. However, the impact strength model increased the simulation time beyond 500 hours, which was deemed unreasonable. Therefore, due to a lack of required computing power to bring this simulation time to a reasonable value, the impact analysis submodel was disregarded for the full system optimization. Instead, the results of the wind load strength submodel were assumed to be a reasonable approximation of the results from impact strength. This is supported by the results from the individual subsystem optimizations. Percent differences between the optimized variables are shown below in Table 7.1.1. At the very least, the two submodels could be expected to demonstrate similar pareto-optimal behavior.

Table 7.1.1. Optimized variables for strength and impact strength submodels.

Variable	Value (Strength)	Value (Impact Strength)	% Difference
w (mm)	60	65	8
h (mm)	30	17	55
t (mm)	2.906	2.906	0
N	5	4	22

7.2 Results

Pareto-optimal points were generated using separate optimizations of three models corresponding to $N = 4, 5$, and 6 ribs. These points, and the second-order pareto-optimal surface, are shown in Figures 7.2.1 and 7.2.2 below.

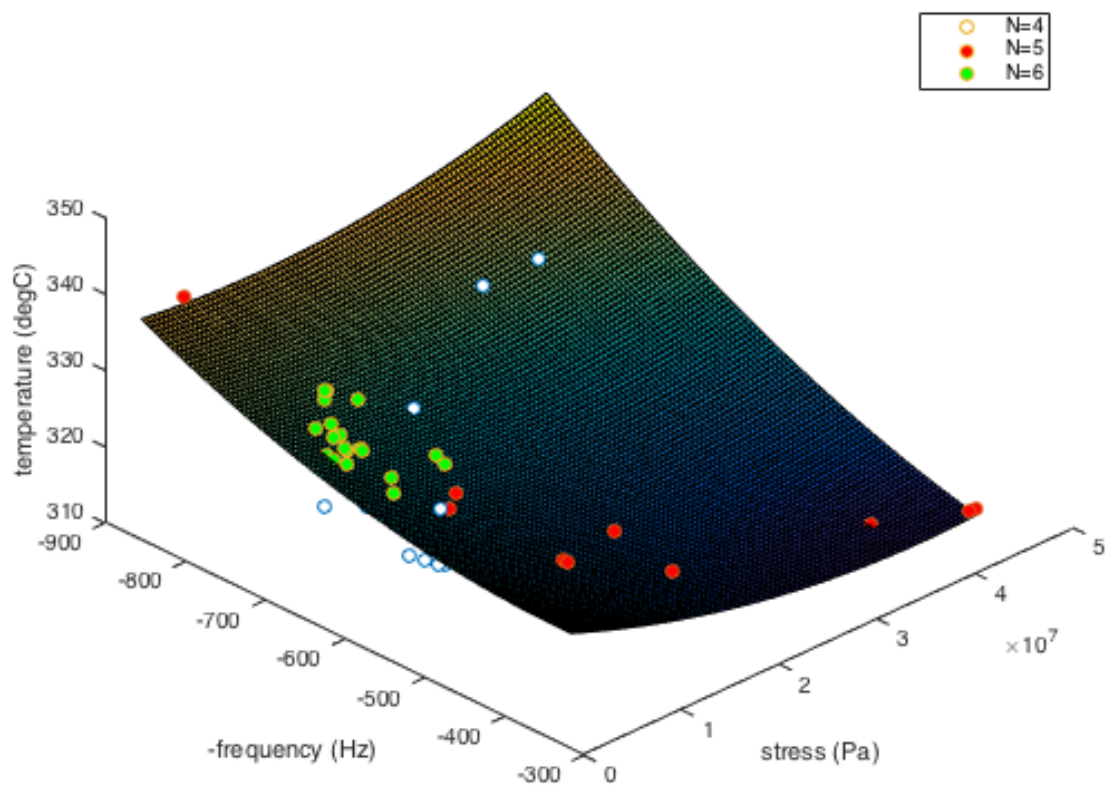


Figure 7.2.1. Isometric view of pareto-optimal surface.

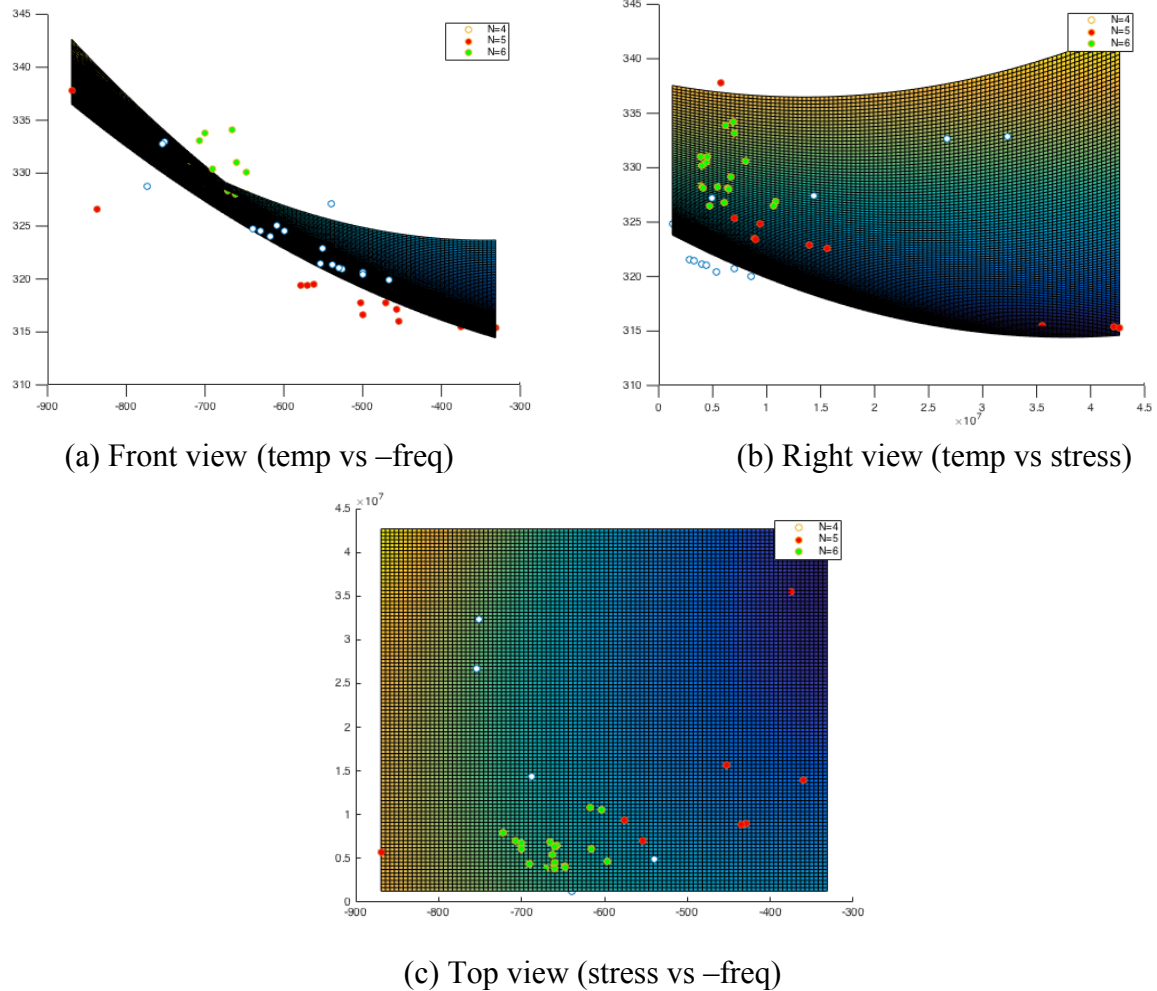


Figure 7.2.2. Two-dimensional views of pareto-optimal surface.

Clearly the points cannot be well approximated by a second-order surface, but as mentioned above, more accurate methods like Kriging did not result in surfaces that showed meaningful trends. In addition, higher-order surfaces did not significantly improve the accuracy of the surface. Therefore, a second-order surface was deemed sufficient.

Interestingly, the different numbers of ribs generated unique patterns of pareto-optimal points, with $N = 6$ generating a very tight cluster of points. Overall, though, the trends are similar and sensible. Stress and frequency can be more or less simultaneously optimized, which makes sense because strength and stiffness are approximately proportional. However, optimizing thermal performance sacrifices both of the other objectives because minimum thermal resistance requires thin geometry, while maximizing strength and natural frequency requires thicker, stiffer geometry. Therefore, no single point will optimize all three objectives. Instead, a design decision should be made based on relative weights of the objectives.

8 Conclusions

The optimized fundamental natural frequency of the panel was 809 Hz, which is well outside the range of helicopter engine performance. This is also a 670% improvement compared to a plain, flat panel. The thermal analysis attempted to minimize the average surface temperature of the panel, as this was seen to be equivalent to maximizing its ability to reject heat from the engine. The optimized design had an average surface temperature of 307°C, which was a 2.04% improvement upon a flat panel design. The panel design optimized for wind load strength had a maximum stress of just 3.4 MPa, which is well below the yield stress of the material. This was a 651% improvement over a flat panel design. The panel design optimized for impact strength demonstrated a maximum stress of 3.4 GPa, which is well above the yield strength of the material. The simulation was not refined to bring this value below the yield stress, because optimization was the focus of the project. In addition, this was still a 632% improvement over a flat panel design.

The system optimization demonstrated that a utopia point does not exist; that is, no panel design will simultaneously optimize all four objective functions. Instead, pareto-optimal surfaces show the tradeoffs between the objectives. These surfaces could be used to make a decision on the design of the panel for its application based on relative weights of the objective functions. Because there is not a substantial change in the panel's thermal performance, this objective should likely be weighted the lowest. And because helicopter engines rotate with maximum frequencies of about 350 Hz, this objective could be compromised down to about 400 Hz with no noticeable impact on its vibration performance.

Overall, ANSYS is a useful tool for design optimization. In particular, response surface optimization is efficient when dealing with manufacturable values of a variable. However, one of ANSYS's most significant limitations is an inability to set the instances of a patterned feature as a design variable. For this, a binary search is a reasonable workaround when the domain of this variable is limited to a reasonably small set of discrete values. Another primary drawback is that the computational power required to perform a system optimization that balances several objective functions quickly becomes unreasonable. For this, there seems to be a reasonable workaround except to eliminate the submodel requiring the most computational power. In this project, assumptions were made that the strength and impact strength submodels had similar pareto-optimal behavior, so the impact strength submodel was deleted without significant consequences. But this is not a heuristic that can be used in a broad variety of situations.

9 References

- [1] Yang, Y., Xia, Z., Zhao, X., Tokura, S., & Hagiwara, I. (2012). Comprehensive Optimization for Raised Floor Structure Using Origami Engineering. *Communications in Computer and Information Science*, 326, 216-227. doi:10.1007/978-3-642-34381-0_26
- [2] Sheet Metal Gauge Size Chart. (n.d.). Retrieved April 20, 2016, from <http://www.custompartnet.com/sheet-metal-gauge>
- [3] Spatz, H., O'leary, E. J., & Vincent, J. F. (1996). Young's Moduli and Shear Moduli in Cortical Bone. *Proceedings of the Royal Society B: Biological Sciences*, 263(1368), 287-294. doi:10.1098/rspb.1996.0044
- [4] Corum, J. (2003, November 17). Estimating the Airspeed Velocity of an Unladen Swallow. Retrieved April 18, 2016, from <http://style.org/unladenswallow/>

10 Appendix

Pareto-optimal points for N = 4, 5, and 6 ribs are shown in the following tables.

Table 10.1. Pareto-optimal points for N = 4 ribs.

Pareto-Optimal Point	Frequency (Hz)	Stress (Pa)	Temperature (deg C)
1	773.397872	6364211.05	328.68213
2	773.618842	6364210.77	328.682129
3	639.483097	1256730.27	324.75243
4	608.555618	3045991.09	325.080785
5	554.32489	2860432.62	321.469147
6	599.183727	3755964.4	324.531631
7	687.950849	14350302.5	327.310397
8	617.046007	10379119	324.011377
9	617.046007	10379119	324.011377
10	629.36281	12017392.3	324.526221
11	538.896638	3261115.95	321.379135
12	530.155758	3984570.8	321.017231
13	526.703464	4418099.93	320.899752
14	551.517702	4629457.92	322.827601
15	500.138735	5292644.9	320.357206
16	499.80781	6961241.11	320.572516
17	753.854771	26689603.5	332.628244
18	467.113761	8587124.64	319.857912
19	539.812343	4951067.07	327.107159
20	751.34996	32291829.6	332.762389

Table 10.2. Pareto-optimal points for N = 5 ribs.

Pareto-Optimal Point	Frequency (Hz)	Stress (Pa)	Temperature (deg C)
1	836.777851	8225815.75	326.507011
2	869.494934	5705229.56	337.747739
3	578.182818	19102688.3	319.316735
4	570.519412	19338537.4	319.321138
5	561.943184	19430844.9	319.444628
6	576.151903	9402793.37	324.783978
7	553.94705	7040733.86	325.244842
8	499.573912	26467289.9	316.541275
9	502.172031	25230610.7	317.658152
10	470.704842	26540860.8	317.619716
11	454.545226	29520547.3	315.903329
12	457.146713	28086052.7	317.012387
13	452.111643	15614952.3	322.458654
14	435.200682	8863743.6	323.349872
15	429.286602	8969013.65	323.263842
16	375.265831	35483177.3	315.315135
17	360.081607	13993822	322.708812
18	333.83499	42184305.5	315.181156
19	331.357184	42677485.8	315.154288

Table 10.3. Pareto-optimal points for N = 6 ribs.

Pareto-Optimal Point	Frequency (Hz)	Stress (Pa)	Temperature (deg C)
1	722.712849	7995557.59	330.5226
2	699.675002	6715784.89	329.061563
3	690.101475	4435404.17	330.3972
4	671.029791	3906022.86	328.294819
5	707.092641	6971415.46	333.081147
6	662.920174	5485496.35	328.10813
7	662.001562	3980765.64	328.029774
8	659.60166	6407832.24	328.005119
9	657.314977	6443018.94	327.935287
10	700.104075	6129479.77	333.787875
11	648.173679	4128186.86	328.053811
12	660.580435	3863430	330.972456
13	660.580435	4538002.71	330.972456
14	647.569753	3948000.56	330.084585
15	647.345957	3950379.23	330.067621
16	616.070425	6096799.81	326.736773
17	616.969398	10785795.8	326.759082
18	666.312838	6859741.12	334.078927
19	603.334517	10576972.8	326.432804
20	596.235044	4720285.23	326.359353

The MATLAB code used to generate a pareto-optimal surface from the above points is shown below. The points for N = 4, 5, and 6 were concatenated to generate a single surface.

pareto3.m

```
clear all; close all; clc;

N4 = xlsread('4 ribs.xlsx',2);
N5 = xlsread('5 ribs.xlsx',2);
N6 = xlsread('6 ribs.xlsx',2);

f_4 = -N4(:,1);
S_4 = N4(:,2);
T_4 = N4(:,3);
f_5 = -N5(:,1);
S_5 = N5(:,2);
T_5 = N5(:,3);
f_6 = -N6(:,1);
S_6 = N6(:,2);
T_6 = N6(:,3);

figure
hold on
scatter3(f_4,S_4,T_4,'MarkerFaceColor','w')
scatter3(f_5,S_5,T_5,'MarkerFaceColor','r')
scatter3(f_6,S_6,T_6,'MarkerFaceColor','g')
legend('N=4','N=5','N=6')
xlabel('-frequency (Hz)')
ylabel('stress (Pa)')
zlabel('temperature (degC)')
rotate3d on

f = [f_4;f_5;f_6];
S = [S_4;S_5;S_6];
T = [T_4;T_5;T_6];
[X1,X2,yhat] = paretoQuad(f,S,T);
surf(X1,X2,yhat)
```

paretoQuad.m

```
function [X1,X2,yhat] = paretoQuad(f,S,T)

X = [f,S];
X(end,:)= [];
y = T;
y(end) = [];
minf = min(f);
maxf = max(f);
minS = min(S);
maxS = max(S);

XX = [X, X.^2, X(:,1).*X(:,2), ones(size(X,1),1)];
beta = (XX'*XX)\(XX'*y);

x1 = [minf:(maxf-minf)/100:maxf];
x2 = [minS:(maxS-minS)/100:maxS];
[X1,X2] = meshgrid(x1,x2);
yhat = zeros(length(x1),length(x2));
for i = 1:length(x1)
    for j = 1:length(x2)
        ff = x1(i);
        SS = x2(j);
        xx = [ff,SS];
        xx = [xx,xx.^2,xx(1)*xx(2),1];
        yhat(j,i)=beta'*xx';
    end
end
end
```